

Chatting with Images for Introspective Visual Thinking

Junfei Wu ^{*12} Jian Guan ^{*3} Qiang Liu ¹² Shu Wu ^{†12} Liang Wang ¹² Wei Wu ^{†3} Tieniu Tan ¹²⁴

Abstract

Current large vision-language models (LVLMs) typically rely on text-only reasoning based on a single-pass visual encoding, which often leads to loss of fine-grained visual information. Recently the proposal of “thinking with images” attempts to alleviate this limitation by manipulating images via external tools or code; however, the resulting visual states are often insufficiently grounded in linguistic semantics, impairing effective cross-modal alignment - particularly when visual semantics or geometric relationships must be reasoned over across distant regions or multiple images. To address these challenges, we propose “chatting with images”, a new framework that reframes visual manipulation as language-guided feature modulation. Under the guidance of expressive language prompts, the model dynamically performs joint re-encoding over multiple image regions, enabling tighter coupling between linguistic reasoning and visual state updates. We instantiate this paradigm in **ViLaVT**, a novel LVLM equipped with a dynamic vision encoder explicitly designed for such interactive visual reasoning, and trained it with a two-stage curriculum combining supervised fine-tuning and reinforcement learning to promote effective reasoning behaviors. Extensive experiments across eight benchmarks demonstrate that **ViLaVT** achieves strong and consistent improvements, with particularly pronounced gains on complex multi-image and video-based spatial reasoning tasks. Code and model are available¹.

1. Introduction

Large Language Models (LLMs) have established new frontiers in complex problem-solving with long-horizon cognition

^{*}Equal contribution ¹NLPR, MAIS, Institute of Automation, Chinese Academy of Sciences ²University of Chinese Academy of Sciences ³Ant Group ⁴Nanjing University. Correspondence to: Shu Wu <shu.wu@nlpr.ia.ac.cn>, Wei Wu <wuwei19850318@gmail.com>.

Preprint. February 13, 2026.

¹<https://github.com/AntResearchNLP/ViLaVT>

tive deliberation (OpenAI, 2024; Guo et al., 2025), demonstrating impressive abilities in domains like mathematics (Wei et al., 2022; Lightman et al., 2023) and software engineering (Chen et al., 2021; Hou et al., 2024). This has motivated to imbue Large Vision-Language Models (LVLMs) with similar cognitive capabilities, aiming to unlock sophisticated multimodal reasoning (Yang et al., 2025d; OpenAI, 2025; Wu et al., 2025b). Despite this progress, the dominant multimodal reasoning paradigm largely adheres to a “thinking about images” workflow (Su et al., 2025c) and remains bottlenecked by single-pass visual encoding: models first produce a fixed set of visual tokens and then conduct subsequent reasoning primarily in the language space (Yang et al., 2025d; Hong et al., 2025). This design implicitly assumes that such static visual tokens can preserve and be fully exploited for rich visual semantics (Huh et al., 2024). In practice, however, task-relevant details can be lost during this compression and further attenuated as reasoning proceeds purely in the textual domain (Huh et al., 2024; Li & Tang, 2024; Wu et al., 2025b). Moreover, this limitation is more pronounced in multi-image spatial reasoning: the common practice of encoding each image independently and aggregating them only in the textual domain obscures geometric relationships across views (Wang et al., 2025b).

To transcend this limitation, recent work has advocated for a paradigm shift towards “thinking with images”, where models interleave textual reasoning with targeted visual manipulations and iteratively re-encode visual inputs to enrich the context with previously lost details (OpenAI, 2025). The attempts in this direction primarily focus on two categories of manipulation: (1) Tool-based manipulation, where the model invokes predefined tools (e.g., image rotation) (Cheng et al., 2024; Qi et al., 2025; Wu et al., 2025b); and (2) Programmatic manipulation, where the model generates executable image processing code (OpenAI, 2025; Zhang et al., 2025d). Despite this conceptual advance, most existing methods still primarily target single-image manipulation. While recent approaches (e.g., ViLASR (Wu et al., 2025b)) can manipulate multiple images within a single reasoning episode, they often encode each view independently and fuse views only in the textual domain, making cross-view geometric alignment difficult. Moreover, the manipulation interface is typically limited to low-level pixel/geometry operations (Wu et al., 2024), which makes it nontrivial to

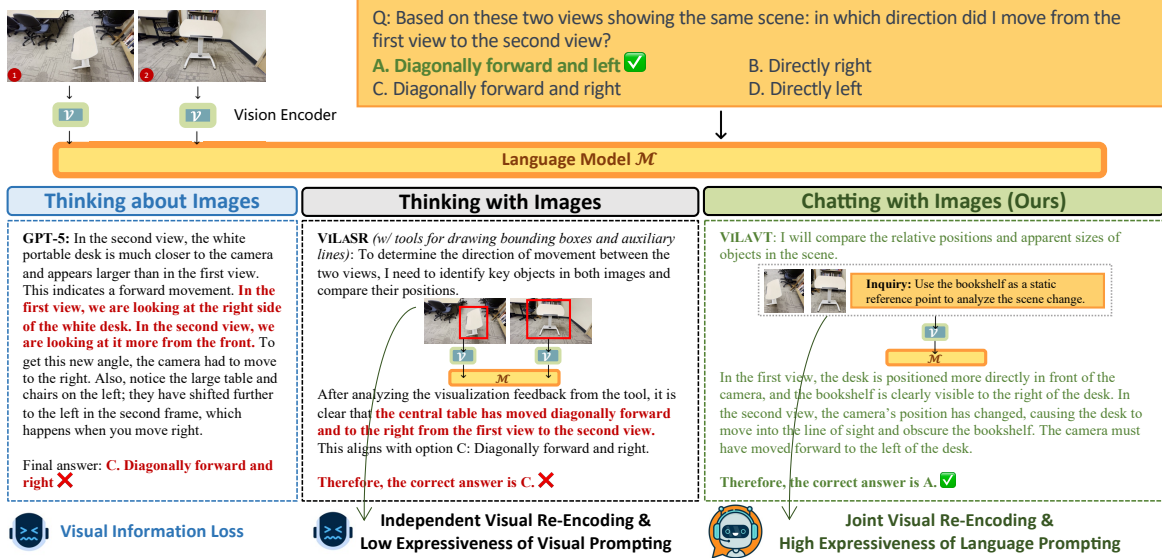


Figure 1. A qualitative comparison of three reasoning paradigms on a multi-view spatial reasoning task. **“Thinking about Images” (Left):** A static LVLM relies on a one-time visual encoding, resulting in information loss. This leads to a flawed understanding of the objects’ spatial relationships and an incorrect answer. **“Thinking with Images” (Center):** This method invokes an external tool to highlight salient information while re-encoding each image independently. However, this visual prompting technique lacks expressiveness and fails to convey the necessary cognitive intent, resulting in a flawed comparison. **“Chatting with Images” (Right):** Our model, in contrast, leverages language prompting. The generated inquiry expresses a high-level cognitive intent. This highly expressive, declarative prompt guides a joint visual re-encoding of both images, enabling a relational comparison at the feature level and leading to the correct inference.

express high-level relational intent. Considering a task like “Find the car that is parked incorrectly”, expressing such high-level relational intent via low-level operations is often cumbersome, requiring a brittle and inefficient chain of operations for detecting cars, lines, and comparing relations. The key challenge is thus to devise a visual manipulation mechanism that is both scalable and expressive, seamlessly bridging high-level intent with low-level feature modulation.

To address these challenges, we propose “chatting with images,” a versatile reasoning paradigm that reframes visual manipulation as language-guided feature modulation (Figure 1). At each reasoning step, the model predicts a set of relevant regions of interest and formulates a natural language inquiry, which serves as a highly expressive language prompt. This declarative prompt leverages the compositional power of language to express complex cognitive intent (e.g., “Use the bookshelf as a static reference”). Instead of triggering external tools, this inquiry directly conditions dynamic, joint encoding over these regions. This process facilitates the model to retrieve fine-grained cues and perform cross-view interactions directly in feature space, thereby alleviating the limitations of independently encoding each view. By leveraging language as a unified control interface, our paradigm reduces reliance on handcrafting a vast combinatorial of specialized tools or program chains.

To realize this paradigm, we develop **ViLAVT**, a novel

Vision-Language model that redefines human-like Visual Thinking. Instead of generating external commands for discrete image operations, ViLAVT learns to introspectively modulate its own visual perception. To this end, we introduce a dynamic vision encoder designed to support this introspective capability. We re-architect the vanilla vision encoder to jointly process multiple, non-contiguous images conditioned on a textual inquiry, enabling cross-view interactions within the encoder instead of late fusion in the textual domain. For training, we first apply supervised fine-tuning (SFT) on a hybrid corpus combining repurposed trajectories from prior tool-/code-based methods with newly synthesized reasoning traces. Following SFT, Reinforcement Learning (RL) elevates the model from an imitator to a strategic problem-solver, enabling it to explore the reasoning space and discover more effective solution pathways.

Extensive experiments show that ViLAVT improves performance over prior paradigms, achieving state-of-the-art results on **5 out of 8** benchmarks with especially strong gains on multi-image and video-based spatial reasoning. Our ablations disentangle the contributions of the reasoning paradigm, vision encoder, and staged training, revealing a monotonic performance lift as these components are progressively integrated. Furthermore, controlled analyses under information-scarce settings show improved detail preservation and stronger cross-view integration, resulting in a **24.8%** performance gain over a vanilla encoder. In

summary, our main contributions are:

- We introduce “chatting with images,” a new reasoning paradigm that reframes visual manipulation as language-guided feature modulation, which mitigates the information loss of static models and the low expressiveness of tool/code-based visual prompting techniques.
- We develop ViLAVT, a novel LVLM featuring a dynamic vision encoder designed to support this paradigm. The encoder is architected to jointly process multiple images conditioned on a language inquiry.
- We demonstrate strong empirical results on 8 benchmarks, achieving state-of-the-art performance on **5/8** of them and consistent improvements across the rest, especially on multi-image and video-based spatial reasoning.

2. Related Works

The evolution of visual reasoning models can be broadly categorized into two dominant paradigms: “thinking about images,” which treats reasoning as a post-perception textual process, and the emerging “thinking with images,” which reconceptualizes vision as an interactive component of the reasoning loop itself. In this section, we review key works within both paradigms.

2.1. Thinking about Images

Most state-of-the-art LVLMs (Liu et al., 2024a; Li et al., 2024a; Bai et al., 2025) operate under the “thinking about images” paradigm. Architecturally, these models process an image once with a powerful visual encoder (Dosovitskiy et al., 2021; Tschannen et al., 2025; Fini et al., 2025) to generate a set of visual embeddings. To bridge the modality gap, these visual embeddings are projected into the language embedding space, typically through a bottleneck mechanism like a small number of learnable query tokens (Li et al., 2023) or a simple linear projection layer (Liu et al., 2024b). The resulting features are then treated as a static “visual prefix” for an LLM, which performs all subsequent reasoning. The LVLMs’ capabilities can be improved through extensive training phases, including supervised fine-tuning (SFT) on instruction-following datasets (Liu et al., 2024b), reinforcement learning from human feedback (RLHF) to align with human preferences (Sun et al., 2023; Yu et al., 2024; Zhang et al., 2025c), and reinforcement learning with verifiable reward (RLVR) to enhance the reliability of long-horizon reasoning (Yang et al., 2025d; Hong et al., 2025; Feng et al., 2025a;b). Despite their impressive performance, the core bottleneck of this paradigm is the irreversible loss of information. This is rooted in the aggressive compression required to map high-dimensional, noisy visual data into a manageable sequence of tokens for the LLM, inevitably leading to the loss of fine-grained details and spatial nuances

before any reasoning occurs.

2.2. Thinking with Images

More recent work has begun to explore the “thinking with images” paradigm (OpenAI, 2025; Su et al., 2025c), aiming to create an interactive reasoning process. These approaches primarily manifest in three categories: (1) **Tool-based manipulation**, where the model dynamically invokes external tools to manipulate the visual input during reasoning (Cheng et al., 2024; Wu et al., 2025b; Zheng et al., 2025; Su et al., 2025b). However, the black-box nature of the tools prevents end-to-end optimization with the model, and a pre-defined and often narrow toolset fundamentally limits the model’s ability to generalize. (2) **Programmatic manipulation**, where the model functions as a visual programmer, generating executable scripts for custom image manipulation (Gupta & Kembhavi, 2023; Surís et al., 2023; Zhang et al., 2025d). While theoretically Turing-complete, this paradigm is hindered by practical issues: high latency from the code generation-execution loop and poor expressiveness limited by pixel-level manipulation. (3) **Generative imagination**, which leverages a model’s internal generative capacity to synthesize new visual images as intermediate thoughts (Li et al., 2025; Chern et al., 2025; Zhang et al., 2025a). However, this approach is not only computationally prohibitive but, more critically, risks ungrounded reasoning, as the synthesized content is generated from the model’s internal priors rather than extracted from the source data. Our work, in contrast, offers a single, unified framework that is both scalable and expressive, leveraging language’s compositional power to articulate cognitive intent beyond any fixed toolset, while simultaneously addressing cross-view information loss through dynamic, joint feature modulation.

3. Methodology

We formulate the visual reasoning task as follows: Given a question Q and a visual input $\mathcal{I} = \{\mathcal{I}_n\}_{n=1}^N$ (where $N = 1$ for a single image and $N > 1$ for a video or image sequence), our goal is to generate the final answer A by producing a reasoning trajectory τ interleaving textual thought and visual manipulation. To achieve this, we introduce the “chatting with images” reasoning paradigm (§3.1), which is underpinned by a novel dynamic vision encoder (§3.2) and a two-stage training strategy, covering SFT (§3.3) and RL (§3.4). Figure 2 and Figure 3 illustrate the model architecture and the training pipeline, respectively.

3.1. The “Chatting with Images” Paradigm

Our framework unifies visual reasoning as a process of generating a trajectory $\tau = (s_1, s_2, \dots, s_T)$, where each step s_t is a triplet $s_t = (r_t, q_t, z_t)$. The components are defined as:

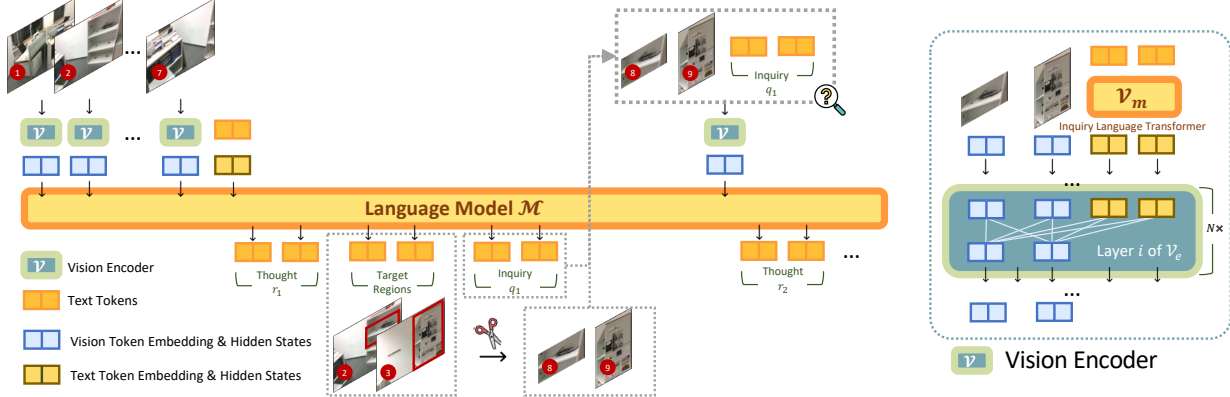


Figure 2. Left: The iterative reasoning process of ViLAVT; **Right:** the architecture of the dynamic vision encoder. The “chatting with image” reasoning paradigm unfolds as: (1) **Initial Encoding:** All input images/frames are initially encoded independently into vision token embeddings. (2) **Stepwise Reasoning:** The language model generates a triplet $s_t = (r_t, q_t, z_t)$, i.e., an internal thought, a natural language inquiry for visual re-encoding, and a set of target regions. (3) **Targeted Re-encoding:** Our dynamic vision encoder (**Right**) takes the textual inquiry q_t and the specified visual regions (cropped and up-scaled from source images/frames) as input, which employs a hybrid attention strategy to jointly process vision and text tokens, producing re-encoded vision token embeddings. (4) **Iteration:** These newly generated vision token embeddings are then passed back to the language model, enriching its context and enabling it to generate the next, more informed reasoning (s_{t+1}). This iteration continues until a final answer is reached.

- r_t : The model’s textual reasoning process.
- q_t : A textual inquiry that directs the vision encoder to perform a targeted re-computation of visual features.
- z_t : A set of target visual regions, formally $z_t = \{(n_t^i, b_t^i)\}_{i=1}^{M_t}$. Here, n_t^i is an index referencing a visual source, which can be an original image or any image produced in a preceding step. The term b_t^i denotes a bounding box that specifies a sub-region to re-examine.

Following the generation of step s_t , the framework crops the set of visual regions \mathcal{C}_t specified by z_t from the preceding images. To enhance detail, each region is up-scaled by a factor of 2 (capped at the original image dimensions) before being fed into the vision encoder \mathcal{V} . The encoder then jointly processes the textual inquiry q_t and the up-scaled regions \mathcal{C}_t to produce a new feature set: $f_t = \mathcal{V}(\mathcal{C}_t, q_t)$. These resulting features f_t are subsequently provided as input to the language model component, which we denote as \mathcal{M} , to inform the generation of the next step s_{t+1} . This iterative process is formally described as:

$$s_{t+1} \sim \mathcal{M}(\cdot \mid f_0, Q, \{(s_k, f_k)\}_{k=1}^t) \quad (1)$$

where $f_0 = \mathcal{V}(\mathcal{I}, \emptyset)$ represents the initial full-frame encoding, and the set $\{(s_k, f_k)\}_{k=1}^t$ constitutes the complete reasoning history up to the current step.

3.2. The Architecture of the Vision Encoder

A vanilla vision encoder (Bai et al., 2025) processes each input image \mathcal{I}_n independently. It first partitions the image into a sequence of patches, which are then linearly projected

into patch embeddings \mathbf{P} . These embeddings are finally encoded by a vision Transformer (Dosovitskiy et al., 2021) to produce the visual representation.

In contrast, the realization of our reasoning paradigm is predicated on a vision encoder with two key capabilities: (1) interpreting a textual inquiry q , and (2) jointly processing a variable number of potentially non-contiguous image regions. To fulfill these requirements, we re-architect the input stage of the vision encoder. Formally, given a set of U images $\mathcal{C} = \{i_u\}_{u=1}^U$ and a textual inquiry q , the operation of our dynamic vision encoder \mathcal{V} is formulated as:

$$\mathcal{V}(\mathcal{C}, q) = \mathcal{V}_e(\mathbf{P}_1 \oplus \mathbf{P}_2 \oplus \dots \oplus \mathbf{P}_U \oplus \mathbf{h}_q), \quad (2)$$

$$\mathbf{h}_q = \mathcal{V}_m(q), \quad (3)$$

where \mathcal{V}_e is a vision Transformer and \mathcal{V}_m is a lightweight language Transformer. Each image i_u is projected into its patch embeddings \mathbf{P}_u . The inquiry q is concurrently encoded by \mathcal{V}_m into a query embedding \mathbf{h}_q . These embeddings are then concatenated (denoted by \oplus), to form a unified input sequence. A left-to-right sequence of 2D positional embeddings (Bai et al., 2025) is applied to this entire sequence, ensuring spatial and semantic coherence across all modalities. This elegant design enables the architecture to gracefully degenerate into a vanilla vision encoder when processing a single image without an inquiry ($U = 1, q = \emptyset$). In contrast to InstructBLIP (Li et al., 2023), which uses a small set of learnable query tokens to query and compress dense visual features into a compact representation, our design enables query-guided cross-region interactions over multiple visual inputs during visual feature extraction.

Within the vision Transformer \mathcal{V}_e , we employ a hybrid atten-

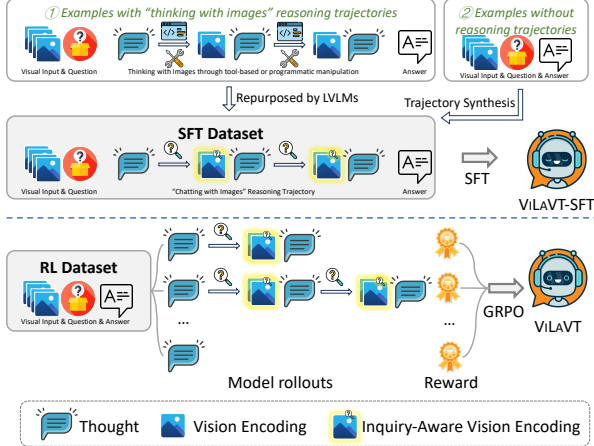


Figure 3. The two-stage training pipeline for VILAVT, including supervised fine-tuning (SFT, Top), followed by reinforcement learning with the GRPO algorithm (RL, Bottom).

tion strategy balancing computational cost and expressive power (Bai et al., 2025): in designated interaction layers, full self-attention is applied across all visual tokens, which also attend to the textual inquiry; in other layers, attention is restricted to operate either within each patch window independently or across the entirety of a single image, but not across distinct images.

3.3. Supervised Fine-tuning

The goal of SFT is to bootstrap the model’s ability to reason within the “chatting with images” paradigm by learning from expert demonstrations. To this end, we construct a large-scale, multi-domain dataset, \mathcal{D}_{SFT} , with reasoning trajectories from two distinct components. Table 4 shows the overview of the training dataset. Appendix A illustrates the data collection process in detail.

The first component is constructed by repurposing existing “thinking with images” datasets featuring either tool-based or programmatic manipulation from the general domain. Since natural language serves as a universal interface capable of abstracting the functionality of any specialized tool or code block, we prompt a powerful teacher LLM to translate each external action—be it a tool call (Wang et al., 2025a) or a code block (Zhang et al., 2025d)—into an action triplet comprising the textual thought, a corresponding natural language inquiry, and the target visual regions. This process effectively unifies the heterogeneous landscape of interactive methods into our native “chatting with images” format.

The second SFT data component targets complex spatial reasoning datasets (Zhang et al., 2025b; Ouyang et al., 2025; Feng, 2025), which requires models to deduce intricate spatial and temporal relationships through deliberate visual

thinking but lacks annotations of reasoning trajectories. The common practice to address this is rejection sampling (Touvron et al., 2023), where a teacher LLM generates entire reasoning trajectories which are then filtered based on the final outcome. However, we argue this method is sub-optimal, as a teacher model’s static visual encoder cannot produce the text-conditioned, multi-region manipulations. Therefore, we design a dedicated pipeline that first programmatically mines latent spatial knowledge by performing parallel analyses (e.g., object grounding, camera motion estimation). This multi-faceted context is then synthesized into high-quality “chatting with images” trajectories, teaching our model to perform nuanced visual reasoning.

In addition, we augment the SFT dataset with purely textual trajectories generated via rejection sampling, teaching the model to answer simple questions efficiently when the visual information is self-evident (Yang et al., 2025b). We then train the model, denoted as π_θ , on this combined dataset via a standard maximum likelihood objective:

$$\mathcal{L}_{\text{SFT}} = -\mathbb{E}_{(\mathcal{I}, Q, \{s_t\}_{t=1}^T) \sim \mathcal{D}_{\text{SFT}}} \sum_{t=1}^T \log \pi_\theta(s_t \mid \mathcal{I}, Q, s_{<t}). \quad (4)$$

3.4. Reinforcement Learning

After SFT, we employ RL to explore the vast reasoning space and directly optimize for task outcomes.

Reward Function. We evaluate each rollout trajectory using an outcome-based reward function:

$$R(\tau) = \mathbb{1}(R_{\text{correct}} > 0)(R_{\text{correct}} + R_{\text{format}}), \quad (5)$$

First, the primary reward R_{correct} measures the answer correctness, and the format reward R_{format} evaluates the syntactic validity of the trajectory. The overall reward implements a strict gating mechanism based on the correctness of the final answer, which ensures the model cannot accumulate reward by generating syntactically perfect but ultimately incorrect reasoning paths (Wu et al., 2025b).

Specifically, the correctness reward, R_{correct} , is computed based on the task type, with a focus on tasks that have verifiable outcomes, including multiple-choice and numerical questions. For multiple-choice questions, R_{correct} is a binary score (1/0) for an exact match. For numerical questions, we employ the Mean Relative Accuracy (MRA) (Yang et al., 2024) to provide a more granular signal. The format reward, R_{format} , is 1 if the entire trajectory is well-parsed and all bounding boxes are syntactically valid; otherwise, it is 0.

Optimization Object. We optimize the policy π_θ using GRPO (Shao et al., 2024), a robust policy gradient algorithm

without the KL penalty term (Hu et al., 2025):

$$\mathcal{L}_{\text{RL}} = -\mathbb{E}_{\tau \sim \pi_\theta} \left[\sum_{t=1}^T \min(\rho_t A(\tau), \text{clip}(\rho_t, 1 - \epsilon_1, 1 + \epsilon_2) A(\tau)) \right],$$

where $\rho_t = \frac{\pi_\theta(a_t|s_t)}{\pi_{\text{old}}(a_t|s_t)}$ and $A(\tau) = \frac{R(\tau) - b}{\sigma + \delta}$. (6)

Here, ρ_t is the importance sampling ratio, and $A(\tau)$ is the advantage computed by normalizing the trajectory reward $R(\tau)$ against the mean (b) and standard deviation (σ) of rewards from a batch of G rollouts, with a small constant δ for numerical stability.

4. Experiments

4.1. Experimental Setup

Evaluation Benchmarks and Metrics. To comprehensively evaluate our model’s capabilities, we select a diverse suite of benchmarks spanning different reasoning complexities and task formats:

- **General visual question-answering (VQA):** This category of tasks assesses the fundamental ability for real-world fine-grained perception and understanding, including *HRBench-4K* and *HRBench-8K* (Wang et al., 2025d).
- **Spatial Reasoning:** This suite is designed to probe the model’s understanding of complex spatial relationships across diverse visual modalities. It is organized into three categories: (i) **single-image** reasoning: *SpatialEval-Real* (Wang et al., 2024) and *EmbSpatial* (Du et al., 2024); (ii) **multi-image** reasoning: *ERQA* (Team et al., 2025), *SPAR-Bench* (Zhang et al., 2025b), and *MMSI-Bench* (Yang et al., 2025c); and (iii) **video-based** reasoning: *VSI-Bench* (Yang et al., 2024).

For evaluation metrics, we report **Accuracy (Acc.)** and **Mean Relative Accuracy (MRA)** (Yang et al., 2024) for multiple-choice and numerical questions, respectively. Appendix B shows the benchmark statistics.

Implementation Details. Our model architecture is initialized from Qwen2.5-VL-7B (Bai et al., 2025). The lightweight language Transformer \mathcal{V}_m in our vision encoder is initialized from Qwen3-0.6B-Embedding (Yang et al., 2025a) and kept frozen during training. During the training phase, we allocate a total budget of 8,192 visual tokens across the initial visual inputs to set each image’s maximum resolution, which is then kept fixed throughout multi-turn reasoning; for video tasks, we uniformly sample 32 frames per clip. For supervised training stage, we train the model for 2 epochs with a learning rate of 1×10^{-5} and a global

batch size of 384. The subsequent RL optimization is implemented using the VERL framework (Sheng et al., 2024), where we set the rollout batch size to 96 and generate 4 candidate reasoning paths per query. Additional details are provided in the Appendix C. We also present the training dynamics in Section D.1.

Baselines. We compare ViLAVT against a comprehensive set of baselines spanning distinct reasoning paradigms:

- **Non-thinking:** The models generate the final answer in a single step without producing an explicit reasoning chain. We include the powerful open-source LVLMs, Qwen2.5-VL (Bai et al., 2025), InternVL3 (Zhu et al., 2025), and LLaVA-OneVision (Li et al., 2024b).
- **Thinking about images:** The models perform textual reasoning to deduce the final answer based on a one-pass, static visual encoding, including Qwen2.5-VL (Bai et al., 2025) and two specialized models for spatial reasoning, i.e., SpaceR (Ouyang et al., 2025) and Spatial-MLLM (Wu et al., 2025a).
- **Thinking with images:** We evaluate against four representative approaches: ViLASR (Wu et al., 2025b), Pixel-Reasoner (Su et al., 2025a) and DeepEyes (Zheng et al., 2025), which leverage external tools for visual manipulation, and Thyme (Zhang et al., 2025d), which generates Python code for programmatic manipulation.

4.2. Main Results

Table 1 shows the main results, highlighting three clear conclusions: (1) **Prior paradigms exhibit task-specific specialization.** Models in both “thinking about images” and “thinking with images” paradigms often excel in narrow domains. For example, Thyme and DeepEyes lead on HRBench but perform weakly on complex spatial reasoning. Conversely, SpaceR and Spatial-MLLM, which are specialized for spatial tasks, lag on general VQA. Such specialization often stems from a lack of a unified and expressive interface for visual interaction, forcing model designs to be narrowly tailored to specific task structures. (2) **“Chatting with images” achieves superior versatility and overall performance.** ViLAVT demonstrates remarkable versatility. It establishes new state-of-the-art results on 5 of 8 benchmarks, particularly in complex multi-image and video-based spatial reasoning. While highly specialized models like Thyme may achieve slightly higher scores on certain single-image VQA tasks, ViLAVT remains highly competitive. By unifying visual interaction within a language-guided framework, ViLAVT emerges as a more powerful and general-purpose visual reasoner. Additionally, Appendix D.2 provides an analysis of the computational overhead introduced by these reasoning paradigms.

Table 1. Main results comparing ViLAVT against baselines across a comprehensive suite of benchmarks. We report accuracy (%) and highlight the best performance in **bold**; the second-best is underlined.

Model	General VQA		Spatial Reasoning					
	Single-Image		Single-Image		Multi-Image			Video
	HRBench-4K	HRBench-8K	SpatialEval-Real	EmbSpatial	ERQA	SPAR-Bench	MMSI-Bench	VSI-Bench
Non-Thinking								
Qwen2.5-VL-7B	67.8	65.1	58.5	52.7	39.3	36.9	26.9	34.7
InternVL3-8B	70.8	62.0	62.3	66.9	35.3	36.0	25.7	42.1
LLaVA-OneVision-7B	64.3	59.8	62.9	72.5	30.6	32.4	24.5	32.4
Thinking about Images								
Qwen2.5-VL-7B	69.8	64.9	54.1	58.2	39.8	31.6	27.1	26.2
SpaceR-7B	58.1	49.8	62.7	<u>69.4</u>	40.3	37.1	28.8	45.6
Spatial-MLLM-4B	-	-	-	-	38.3	35.1	27.7	<u>48.4</u>
Thinking with Images								
ViLASR-7B	60.5	56.3	<u>63.9</u>	66.4	41.0	37.6	<u>30.2</u>	45.4
Pixel-Reasoner-7B	72.9	66.9	61.6	62.3	-	-	-	-
DeepEyes-7B	75.1	72.6	62.8	64.2	-	-	-	-
Thyme-7B	78.3	<u>72.4</u>	63.7	65.5	-	-	-	-
Chatting with Images (Ours)								
ViLAVT-7B	<u>75.5</u>	69.3	68.9	69.3	42.2	52.6	31.3	52.0

Table 2. Ablation study on training stages and model components.

Model	HRBench-4K	HRBench-8K	ERQA	VSI-Bench
Qwen2.5-VL-7B	67.8	65.1	39.3	34.7
Qwen2.5-VL-7B-SFT	68.8	63.6	38.8	46.9
ViLAVT-SFT	73.6	66.1	39.8	43.3
ViLAVT	75.5	69.3	42.2	52.0
ViLAVT ₄₀₀ w/ vanilla ViT	73.3	65.7	40.3	47.4
ViLAVT ₄₀₀	73.4	67.0	40.7	49.0

4.3. Ablation Studies on Training Stages and Model Components

To validate our design choices, we conduct ablation studies on five variants: (1) **Qwen2.5-VL-7B**: the base model; (2) **Qwen2.5-VL-7B-SFT**: the base model SFT-trained on the same corpus using only question–answer pairs with no reasoning chains; (3) **ViLAVT-SFT**: our model trained with SFT only; Additionally, to isolate the contribution of our dynamic vision encoder, we train two variants with the same full SFT stage and 400-step RL schedule, in contrast to full 1200-step RL stage for ViLAVT: (4) **ViLAVT₄₀₀ w/ vanilla ViT**, which replaces our dynamic encoder with a standard ViT, and (5) **ViLAVT₄₀₀**, which retains the full model architecture but trains the RL stage for only 400 steps. The results in Table 2 reveal several key insights:

Importance of our paradigm. Comparing Qwen2.5-VL-7B-SFT with ViLAVT trained on the same corpus, Qwen2.5-VL-7B-SFT yields only a modest 1.0% on HRBench-4K and even drops on HRBench-8K relative to the base model. In contrast, ViLAVT consistently outperforms Qwen2.5-VL-7B-SFT, showing that the gains mainly stem from our framework rather than data scaling alone.

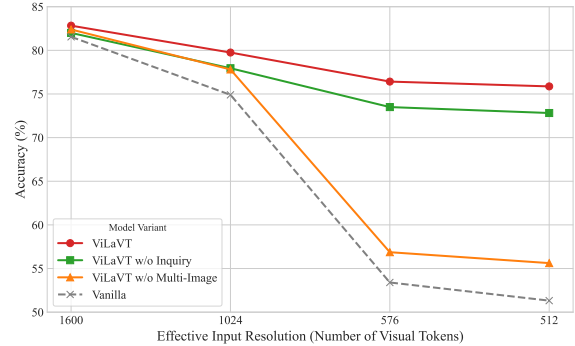


Figure 4. Vision encoder analysis across resolutions. Our full model exhibits increasingly performance gains over ablations as resolutions decreases, evidencing robustness to information loss.

Importance of training stages. ViLAVT-SFT achieves substantial improvements over the base model, indicating that supervised fine-tuning effectively enables the model to acquire the proposed interactive format. Building upon this foundation, ViLAVT further improves over ViLAVT-SFT across all benchmarks, suggesting that RL refines the model’s interactive reasoning beyond supervised learning.

Importance of our vision encoder. Under the same full SFT + 400-step RL training schedule, we observe that ViLAVT₄₀₀ consistently outperforms ViLAVT₄₀₀ w/ vanilla ViT, especially on HRBench-8K and VSI-Bench, indicating that the gains come not only from iterative reasoning but also from query-conditioned joint encoding within our vision encoder.

Table 3. Ablations on *HRBench-4K* across image resolutions.

Input Resolution	Qwen2.5-VL-7B	ViLAVT-SFT	ViLAVT
1024	56.4	62.5	63.9
2048	61.4	69.8	70.1
4096	66.8	69.9	73.0
8192	67.8	73.6	75.5

4.4. Analysis under Different Resolutions

To isolate and validate the effectiveness of our dynamic vision encoder, we first conduct a controlled experiment on a subset of the SPAR dataset (Zhang et al., 2025b), comprising 6,489 training and 721 testing examples, each with 2-4 associated images. All models are trained on this subset for 5 epochs to directly predict the final answer, bypassing any textual reasoning chain. The training for all models used a fixed maximum input resolution of $1600 \times 28 \times 28$ pixels, corresponding to 1600 visual tokens. We compare ViLAVT with three ablations: (1) **ViLAVT w/o Inquiry**, removing inquiry-conditioning; (2) **ViLAVT w/o Multi-Image**, removing multi-image interaction; and (3) **Vanilla**, removing both. As shown in Figure 4, performance drops as resolution decreases for all models, but ViLAVT remains substantially more robust; at 512 tokens, it achieves 75.9% accuracy creating a 24.8% performance gap over the vanilla model’s 51.1%. The ablations further suggest that joint multi-image encoding is the main driver of robustness on this multi-view benchmark, while inquiry-conditioning provides a consistent additional gain. These results that our architectural modifications are critical for preserving performance in information-scarce scenarios².

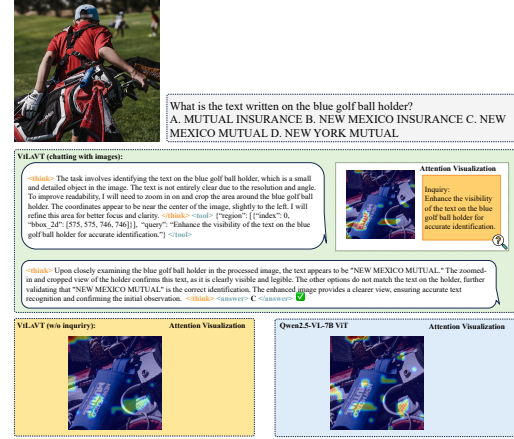
To validate the generalizability of these findings, we further evaluate ViLAVT on *HRBench-4K* under varying token budgets (Table 3). ViLAVT consistently outperforms the base Qwen2.5-VL-7B across all resolutions, including information-scarce settings (e.g., 63.9% vs. 56.4% at 1,024 tokens). Moreover, the performance gap between ViLAVT-SFT and the full ViLAVT persists across resolutions, demonstrating that RL refines the model’s reasoning strategy under different resolution constraints.

4.5. Case Study

4.5.1. REPRESENTATIVE CASE

Figure 10 qualitatively demonstrates our paradigm’s strength on a complex video-based spatial reasoning task. ViLAVT successfully solves the problem by using highly

²Although effective for static multi-view inputs, this single-pass encoding is computationally prohibitive for long videos and structurally unsuited for multi-hop reasoning. Therefore, our main experiments employ the full iterative paradigm, which starts with a vanilla visual encoding and then performs dynamic, targeted re-encoding during reasoning to balance performance with scalability.

Figure 5. Attention visualization on an *HRBench-4K* example.

expressive language prompts to express clear cognitive intent, which then guide a joint, relational re-encoding of features across key frames (e.g., comparing Images 25-27 against Image 5). This enables the model to build a coherent spatial map. We provide further comparisons with other “thinking with images” methods in Appendix E.

4.5.2. ATTENTION MAP VISUALIZATION

Figure 5 illustrates that inquiry-conditioned encoding yields sharper attention on task-relevant regions. Conditioned on the textual inquiry, ViLAVT progressively focuses on task-relevant regions—first localizing the blue golf ball holder, then focus on its embedded text during re-encoding. In contrast, ViLAVT w/o Inquiry and Qwen2.5-VL-7B with a vanilla ViT backbone exhibit more diffuse attention. This qualitative evidence supports that conditioning the vision encoder on the inquiry improves localized perception and facilitates fine-grained detail extraction. Additional cases and visualization details are provided in Appendix E.2.

5. Conclusion

In this work, we introduce “chatting with images,” a unified and scalable visual reasoning paradigm designed to overcome the dual limitations of modern approaches: the information loss in static “thinking about images” and the low expressiveness of visual prompts within “thinking with images”. We reframe visual manipulation as language-guided feature modulation, bridging high-level declarative intent, articulated through expressive language prompts, with deep relational analysis enabled by joint feature re-encoding. Comprehensive experiments validate the superiority of our approach, which establishes new state-of-the-art results on most evaluated benchmarks. Looking ahead, we believe this paradigm opens promising avenues for developing more compositional and general-purpose visual reasoning agents.

Impact Statement

This work aims to improve the reliability and reasoning capability of large vision–language models by enabling language-guided, multi-turn interaction with visual evidence. If deployed responsibly, such models may benefit applications that require careful visual grounding, such as grounded question answering, education, and scientific or engineering assistance.

References

Bai, S., Chen, K., Liu, X., Wang, J., Ge, W., Song, S., Dang, K., Wang, P., Wang, S., Tang, J., et al. Qwen2. 5-vl technical report. *arXiv preprint arXiv:2502.13923*, 2025.

Chen, M., Tworek, J., Jun, H., Yuan, Q., de Oliveira Pinto, H. P., Kaplan, J., Edwards, H., Burda, Y., Joseph, N., Brockman, G., Ray, A., Puri, R., Krueger, G., Petrov, M., Khlaaf, H., Sastry, G., Mishkin, P., Chan, B., Gray, S., Ryder, N., Pavlov, M., Power, A., Kaiser, L., Bavarian, M., Winter, C., Tillet, P., Such, F. P., Cummings, D., Plappert, M., Chantzis, F., Barnes, E., Herbert-Voss, A., Guss, W. H., Nichol, A., Paino, A., Tezak, N., Tang, J., Babuschkin, I., Balaji, S., Jain, S., Saunders, W., Hesse, C., Carr, A. N., Leike, J., Achiam, J., Misra, V., Morikawa, E., Radford, A., Knight, M., Brundage, M., Murati, M., Mayer, K., Welinder, P., McGrew, B., Amodei, D., McCandlish, S., Sutskever, I., and Zaremba, W. Evaluating large language models trained on code, 2021. URL <https://arxiv.org/abs/2107.03374>.

Cheng, C., Guan, J., Wu, W., and Yan, R. From the least to the most: Building a plug-and-play visual reasoner via data synthesis. In Al-Onaizan, Y., Bansal, M., and Chen, Y.-N. (eds.), *Proceedings of the 2024 Conference on Empirical Methods in Natural Language Processing*, pp. 4941–4957, Miami, Florida, USA, November 2024. Association for Computational Linguistics. doi: 10.18653/v1/2024.emnlp-main.284. URL <https://aclanthology.org/2024.emnlp-main.284/>.

Chern, E., Hu, Z., Chern, S., Kou, S., Su, J., Ma, Y., Deng, Z., and Liu, P. Thinking with generated images. *arXiv preprint arXiv:2505.22525*, 2025.

Dosovitskiy, A., Beyer, L., Kolesnikov, A., Weissenborn, D., Zhai, X., Unterthiner, T., Dehghani, M., Minderer, M., Heigold, G., Gelly, S., Uszkoreit, J., and Houlsby, N. An image is worth 16x16 words: Transformers for image recognition at scale. In *International Conference on Learning Representations*, 2021. URL <https://openreview.net/forum?id=YicbFdNTTy>.

Du, M., Wu, B., Li, Z., Huang, X., and Wei, Z. EmbSpatial-bench: Benchmarking spatial understanding for embodied tasks with large vision–language models. In Ku, L.-W., Martins, A., and Srikumar, V. (eds.), *Proceedings of the 62nd Annual Meeting of the Association for Computational Linguistics (Volume 2: Short Papers)*, pp. 346–355, Bangkok, Thailand, August 2024. Association for Computational Linguistics. doi: 10.18653/v1/2024.acl-short.33. URL <https://aclanthology.org/2024.acl-short.33/>.

Duan, H., Yang, J., Qiao, Y., Fang, X., Chen, L., Liu, Y., Dong, X., Zang, Y., Zhang, P., Wang, J., et al. Vlmevalkit: An open-source toolkit for evaluating large multi-modality models. In *Proceedings of the 32nd ACM international conference on multimedia*, pp. 11198–11201, 2024.

Dubey, A., Jauhri, A., Pandey, A., Kadian, A., Al-Dahle, A., Letman, A., Mathur, A., Schelten, A., Yang, A., Fan, A., et al. The llama 3 herd of models. *arXiv preprint arXiv:2407.21783*, 2024.

Feng, K., Gong, K., Li, B., Guo, Z., Wang, Y., Peng, T., Wang, B., and Yue, X. Video-r1: Reinforcing video reasoning in mllms. *arXiv preprint arXiv:2503.21776*, 2025a.

Feng, K., Zhang, M., Li, H., Fan, K., Chen, S., Jiang, Y., Zheng, D., Sun, P., Zhang, Y., Sun, H., Feng, Y., Pei, P., Cai, X., and Yue, X. Onethinker: All-in-one reasoning model for image and video, 2025b. URL <https://arxiv.org/abs/2512.03043>.

Feng, Q. Visuospatial cognitive assistant. *arXiv preprint arXiv:2505.12312*, 2025.

Fini, E., Shukor, M., Li, X., Dufter, P., Klein, M., Haldimann, D., Aitharaju, S., da Costa, V. G. T., Béthune, L., Gan, Z., et al. Multimodal autoregressive pre-training of large vision encoders. In *Proceedings of the Computer Vision and Pattern Recognition Conference*, pp. 9641–9654, 2025.

Guo, D., Yang, D., Zhang, H., Song, J., Zhang, R., Xu, R., Zhu, Q., Ma, S., Wang, P., Bi, X., et al. Deepseek-r1: Incentivizing reasoning capability in llms via reinforcement learning. *arXiv preprint arXiv:2501.12948*, 2025.

Gupta, T. and Kembhavi, A. Visual programming: Compositional visual reasoning without training. In *Proceedings of the IEEE/CVF Conference on Computer Vision and Pattern Recognition*, pp. 14953–14962, 2023.

Holtzman, A., Buys, J., Du, L., Forbes, M., and Choi, Y. The curious case of neural text degeneration. In *International Conference on Learning Representations*, 2024.

2020. URL <https://openreview.net/forum?id=rygGQyrFvH>.

Hong, W., Yu, W., Gu, X., Wang, G., Gan, G., Tang, H., Cheng, J., Qi, J., Ji, J., Pan, L., et al. Glm-4.1 v-thinking: Towards versatile multimodal reasoning with scalable reinforcement learning. *arXiv e-prints*, pp. arXiv-2507, 2025.

Hou, X., Zhao, Y., Liu, Y., Yang, Z., Wang, K., Li, L., Luo, X., Lo, D., Grundy, J., and Wang, H. Large language models for software engineering: A systematic literature review. *ACM Transactions on Software Engineering and Methodology*, 33(8):1–79, 2024.

Hu, J., Zhang, Y., Han, Q., Jiang, D., Zhang, X., and Shum, H.-Y. Open-reasoner-zero: An open source approach to scaling up reinforcement learning on the base model, 2025. URL <https://arxiv.org/abs/2503.24290>.

Huh, M., Cheung, B., Wang, T., and Isola, P. Position: The platonic representation hypothesis. In *Forty-first International Conference on Machine Learning*, 2024.

Kwon, W., Li, Z., Zhuang, S., Sheng, Y., Zheng, L., Yu, C. H., Gonzalez, J., Zhang, H., and Stoica, I. Efficient memory management for large language model serving with pagedattention. In *Proceedings of the 29th symposium on operating systems principles*, pp. 611–626, 2023.

Li, B., Zhang, Y., Guo, D., Zhang, R., Li, F., Zhang, H., Zhang, K., Zhang, P., Li, Y., Liu, Z., and Li, C. Llava-onevision: Easy visual task transfer, 2024a. URL <https://arxiv.org/abs/2408.03326>.

Li, B., Zhang, Y., Guo, D., Zhang, R., Li, F., Zhang, H., Zhang, K., Zhang, P., Li, Y., Liu, Z., et al. Llava-onevision: Easy visual task transfer. *arXiv preprint arXiv:2408.03326*, 2024b.

Li, C., Wu, W., Zhang, H., Xia, Y., Mao, S., Dong, L., Vulić, I., and Wei, F. Imagine while reasoning in space: Multimodal visualization-of-thought. *arXiv preprint arXiv:2501.07542*, 2025.

Li, J., Li, D., Savarese, S., and Hoi, S. Blip-2: Bootstrapping language-image pre-training with frozen image encoders and large language models. In *International conference on machine learning*, pp. 19730–19742. PMLR, 2023.

Li, S. and Tang, H. Multimodal alignment and fusion: A survey. *arXiv preprint arXiv:2411.17040*, 2024.

Lightman, H., Kosaraju, V., Burda, Y., Edwards, H., Baker, B., Lee, T., Leike, J., Schulman, J., Sutskever, I., and Cobbe, K. Let’s verify step by step. *arXiv preprint arXiv:2305.20050*, 2023.

Liu, H., Li, C., Li, Y., Li, B., Zhang, Y., Shen, S., and Lee, Y. J. Llava-next: Improved reasoning, ocr, and world knowledge, January 2024a. URL <https://llava-vl.github.io/blog/2024-01-30-llava-next/>.

Liu, H., Li, C., Wu, Q., and Lee, Y. J. Visual instruction tuning. *Advances in neural information processing systems*, 36, 2024b.

Loshchilov, I. and Hutter, F. Decoupled weight decay regularization. In *International Conference on Learning Representations*, 2019. URL <https://openreview.net/forum?id=Bkg6RiCqY7>.

OpenAI. Introducing openai o1-preview. <https://openai.com/index/introducing-openai-o1-preview/>, 2024.

OpenAI. Introducing openai o3 and o4-mini, 2025. URL <https://openai.com/index/introducing-o3-and-o4-mini/>.

Ouyang, K., Liu, Y., Wu, H., Liu, Y., Zhou, H., Zhou, J., Meng, F., and Sun, X. Spacer: Reinforcing mllms in video spatial reasoning, 2025. URL <https://arxiv.org/abs/2504.01805>.

Qi, J., Ding, M., Wang, W., Bai, Y., Lv, Q., Hong, W., Xu, B., Hou, L., Li, J., Dong, Y., and Tang, J. Cogcom: A visual language model with chain-of-manipulations reasoning. In *The Thirteenth International Conference on Learning Representations*, 2025. URL <https://openreview.net/forum?id=Fg0eo2AkST>.

Shao, Z., Wang, P., Zhu, Q., Xu, R., Song, J., Zhang, M., Li, Y., Wu, Y., and Guo, D. Deepseekmath: Pushing the limits of mathematical reasoning in open language models. *arXiv preprint arXiv:2402.03300*, 2024.

Sheng, G., Zhang, C., Ye, Z., Wu, X., Zhang, W., Zhang, R., Peng, Y., Lin, H., and Wu, C. Hybridflow: A flexible and efficient rlhf framework. *arXiv preprint arXiv:2409.19256*, 2024.

Su, A., Wang, H., Ren, W., Lin, F., and Chen, W. Pixel reasoner: Incentivizing pixel-space reasoning with curiosity-driven reinforcement learning. *arXiv preprint arXiv:2505.15966*, 2025a.

Su, Z., Li, L., Song, M., Hao, Y., Yang, Z., Zhang, J., Chen, G., Gu, J., Li, J., Qu, X., et al. Openthinkimg: Learning to think with images via visual tool reinforcement learning. *arXiv preprint arXiv:2505.08617*, 2025b.

Su, Z., Xia, P., Guo, H., Liu, Z., Ma, Y., Qu, X., Liu, J., Li, Y., Zeng, K., Yang, Z., et al. Thinking with images for multimodal reasoning: Foundations, methods, and future frontiers. *arXiv preprint arXiv:2506.23918*, 2025c.

Sun, Z., Shen, S., Cao, S., Liu, H., Li, C., Shen, Y., Gan, C., Gui, L.-Y., Wang, Y.-X., Yang, Y., et al. Aligning large multimodal models with factually augmented rlhf. *arXiv preprint arXiv:2309.14525*, 2023.

Surís, D., Menon, S., and Vondrick, C. Vipergpt: Visual inference via python execution for reasoning. In *Proceedings of the IEEE/CVF International Conference on Computer Vision*, pp. 11888–11898, 2023.

Team, G. R., Abeyruwan, S., Ainslie, J., Alayrac, J.-B., Arenas, M. G., Armstrong, T., Balakrishna, A., Baruch, R., Bauza, M., Blokzijl, M., et al. Gemini robotics: Bringing ai into the physical world. *arXiv preprint arXiv:2503.20020*, 2025.

Touvron, H., Martin, L., Stone, K., Albert, P., Almahairi, A., Babaei, Y., Bashlykov, N., Batra, S., Bhargava, P., Bhosale, S., et al. Llama 2: Open foundation and fine-tuned chat models. *arXiv preprint arXiv:2307.09288*, 2023.

Tschannen, M., Gritsenko, A., Wang, X., Naeem, M. F., Alabdulmohsin, I., Parthasarathy, N., Evans, T., Beyer, L., Xia, Y., Mustafa, B., et al. Siglip 2: Multilingual vision-language encoders with improved semantic understanding, localization, and dense features. *arXiv preprint arXiv:2502.14786*, 2025.

Wang, H., Li, X., Huang, Z., Wang, A., Wang, J., Zhang, T., Zheng, J., Bai, S., Kang, Z., Feng, J., Wang, Z., and Zhang, Z. Traceable evidence enhanced visual grounded reasoning: Evaluation and methodology, 2025a. URL <https://arxiv.org/abs/2507.07999>.

Wang, J., Ming, Y., Shi, Z., Vineet, V., Wang, X., Li, Y., and Joshi, N. Is a picture worth a thousand words? delving into spatial reasoning for vision language models. In Globerson, A., Mackey, L., Belgrave, D., Fan, A., Paquet, U., Tomczak, J., and Zhang, C. (eds.), *Advances in Neural Information Processing Systems*, volume 37, pp. 75392–75421. Curran Associates, Inc., 2024. URL https://proceedings.neurips.cc/paper_files/paper/2024/file/89cc5e613d34f90de90c21e996e60b30-Paper-Conference.pdf.

Wang, J., Chen, M., Karaev, N., Vedaldi, A., Rupprecht, C., and Novotny, D. Vggt: Visual geometry grounded transformer. In *Proceedings of the IEEE/CVF Conference on Computer Vision and Pattern Recognition*, 2025b.

Wang, J., Kang, Z., Wang, H., Jiang, H., Li, J., Wu, B., Wang, Y., Ran, J., Liang, X., Feng, C., et al. Vgr: Visual grounded reasoning. *arXiv preprint arXiv:2506.11991*, 2025c.

Wang, W., Ding, L., Zeng, M., Zhou, X., Shen, L., Luo, Y., Yu, W., and Tao, D. Divide, conquer and combine: A training-free framework for high-resolution image perception in multimodal large language models. In *Proceedings of the AAAI Conference on Artificial Intelligence*, pp. 7907–7915, 2025d.

Wei, J., Wang, X., Schuurmans, D., Bosma, M., Xia, F., Chi, E., Le, Q. V., Zhou, D., et al. Chain-of-thought prompting elicits reasoning in large language models. *Advances in Neural Information Processing Systems*, 35: 24824–24837, 2022.

Wu, D., Liu, F., Hung, Y.-H., and Duan, Y. Spatial-mllm: Boosting mllm capabilities in visual-based spatial intelligence. *arXiv preprint arXiv:2505.23747*, 2025a.

Wu, J., Zhang, Z., Xia, Y., Li, X., Xia, Z., Chang, A., Yu, T., Kim, S., Rossi, R. A., Zhang, R., Mitra, S., Metaxas, D. N., Yao, L., Shang, J., and McAuley, J. Visual prompting in multimodal large language models: A survey, 2024. URL <https://arxiv.org/abs/2409.15310>.

Wu, J., Guan, J., Feng, K., Liu, Q., Wu, S., Wang, L., Wu, W., and Tan, T. Reinforcing spatial reasoning in vision-language models with interwoven thinking and visual drawing. *arXiv preprint arXiv:2506.09965*, 2025b.

Yang, A., Li, A., Yang, B., Zhang, B., Hui, B., Zheng, B., Yu, B., Gao, C., Huang, C., Lv, C., et al. Qwen3 technical report. *arXiv preprint arXiv:2505.09388*, 2025a.

Yang, B., Wen, B., Ding, B., Liu, C., Chu, C., Song, C., Rao, C., Yi, C., Li, D., Zang, D., et al. Kwai keye-vl 1.5 technical report. *arXiv preprint arXiv:2509.01563*, 2025b.

Yang, J., Yang, S., Gupta, A., Han, R., Fei-Fei, L., and Xie, S. Thinking in Space: How Multimodal Large Language Models See, Remember and Recall Spaces. *arXiv preprint arXiv:2412.14171*, 2024.

Yang, S., Xu, R., Xie, Y., Yang, S., Li, M., Lin, J., Zhu, C., Chen, X., Duan, H., Yue, X., Lin, D., Wang, T., and Pang, J. Mmsi-bench: A benchmark for multi-image spatial intelligence, 2025c. URL <https://arxiv.org/abs/2505.23764>.

Yang, Y., He, X., Pan, H., Jiang, X., Deng, Y., Yang, X., Lu, H., Yin, D., Rao, F., Zhu, M., et al. R1-onevision: Advancing generalized multimodal reasoning through cross-modal formalization. *arXiv preprint arXiv:2503.10615*, 2025d.

Yu, T., Yao, Y., Zhang, H., He, T., Han, Y., Cui, G., Hu, J., Liu, Z., Zheng, H.-T., Sun, M., et al. Rlhf-v: Towards trustworthy mllms via behavior alignment from

fine-grained correctional human feedback. In *Proceedings of the IEEE/CVF Conference on Computer Vision and Pattern Recognition*, pp. 13807–13816, 2024.

Zhang, H., Wu, W., Li, C., Shang, N., Xia, Y., Huang, Y., Zhang, Y., Dong, L., Zhang, Z., Wang, L., et al. Latent sketchpad: Sketching visual thoughts to elicit multimodal reasoning in mllms. *arXiv preprint arXiv:2510.24514*, 2025a.

Zhang, J., Chen, Y., Zhou, Y., Xu, Y., Huang, Z., Mei, J., Chen, J., Yuan, Y.-J., Cai, X., Huang, G., et al. From flatland to space: Teaching vision-language models to perceive and reason in 3d. *arXiv preprint arXiv:2503.22976*, 2025b.

Zhang, Y., Yu, T., Tian, H., Fu, C., Li, P., Zeng, J., Xie, W., Shi, Y., Zhang, H., Wu, J., Wang, X., Hu, Y., Wen, B., Gao, T., Zhang, Z., Yang, F., ZHANG, D., Wang, L., and Jin, R. MM-RLHF: The next step forward in multimodal LLM alignment. In *Forty-second International Conference on Machine Learning*, 2025c. URL <https://openreview.net/forum?id=ULJ4gJJYFp>.

Zhang, Y.-F., Lu, X., Yin, S., Fu, C., Chen, W., Hu, X., Wen, B., Jiang, K., Liu, C., Zhang, T., et al. Thyme: Think beyond images. *arXiv preprint arXiv:2508.11630*, 2025d.

Zheng, Z., Yang, M., Hong, J., Zhao, C., Xu, G., Yang, L., Shen, C., and Yu, X. Deepeyes: Incentivizing” thinking with images” via reinforcement learning. *arXiv preprint arXiv:2505.14362*, 2025.

Zhu, J., Wang, W., Chen, Z., Liu, Z., Ye, S., Gu, L., Tian, H., Duan, Y., Su, W., Shao, J., et al. Internvl3: Exploring advanced training and test-time recipes for open-source multimodal models. *arXiv preprint arXiv:2504.10479*, 2025.

A. Data Construction

Our Supervised Fine-Tuning (SFT) dataset, \mathcal{D}_{SFT} , is meticulously constructed from three distinct sources to provide our model with a comprehensive and diverse set of reasoning skills. This section details the construction process for each component.

A.1. Component 1: Repurposing “Thinking with Images” Trajectories

The first component is constructed by repurposing existing “thinking with images” datasets from the general domain, which feature either tool-based (Wang et al., 2025a) or programmatic manipulation (Zhang et al., 2025d). The core idea is to translate the procedural, external actions from these datasets into our declarative, internal “chatting with images” format. We leverage the hypothesis that natural language serves as a universal interface capable of abstracting the functionality of any specialized tool or code block.

To achieve this, we prompt a powerful teacher LVLM, Qwen2.5-VL-72B (Bai et al., 2025), to translate each external action (i.e., either a tool call or a code block) into an action triplet comprising (1) the textual thought, (2) a corresponding natural language inquiry, and (3) the target visual regions. The prompt used for this conversion is detailed in Figure 6. This process effectively unifies the heterogeneous landscape of interactive methods into our native format. Figure 8 provides concrete examples of this conversion process.

A.2. Component 2: Synthesizing Spatial Reasoning Trajectories

The second SFT data component targets complex spatial reasoning datasets (Zhang et al., 2025b; Ouyang et al., 2025; Feng, 2025). These datasets require models to deduce intricate spatial and temporal relationships but lack annotated reasoning trajectories. A common practice to address this is rejection sampling (Touvron et al., 2023), where a teacher LVLM generates entire trajectories that are then filtered based on the final answer. We argue this method is sub-optimal for our needs, as a static teacher model cannot produce the rich, text-conditioned, multi-region manipulations that our framework is designed for.

Therefore, we designed a dedicated synthesis pipeline, illustrated in Figure 7, to generate high-quality “chatting with images” trajectories. This pipeline first programmatically mines latent spatial and contextual knowledge before synthesizing the final reasoning path. The steps are as follows:

1. **Input:** The pipeline starts with the initial visual input (images/video) and the user’s question.
2. **Parallel Knowledge Mining:** Several analyses are per-

formed in parallel to extract multi-faceted information:

- **Object detection and grounding:** Based on the question, Qwen2.5-VL-72B identifies all potentially important objects in the scene. For each identified object, Qwen2.5-VL-72B generates its corresponding bounding box (“bbox”) for each frame it appears in.
- **Camera annotation:** We use VGGT (Wang et al., 2025b) to estimate camera motion across input images, providing crucial information about viewpoint changes. This yields a sequence of camera positions.

3. **Holistic Captioning:** Qwen2.5-VL-72B generates a single, comprehensive caption for the entire visual input. This caption describes not only the static objects and their relationships but also the temporal dynamics, such as camera movements between different frames.
4. **Reasoning Generation:** All the mined information, including important objects and their bounding boxes, camera positions, and detailed captions, is consolidated and fed as rich context to Qwen2.5-VL-72B. With this comprehensive understanding of the scene, the model is prompted to generate a high-quality reasoning trajectory (interleaving thoughts and tool calls) and the final answer.
5. **Output:** The final output from this guided process is a complete “chatting with images” trajectory generated by Qwen2.5-VL-72B. This trajectory, which includes the detailed reasoning path and the final outcome, serves as a gold-standard training sample for our model.

This structured, knowledge-first approach ensures the generated trajectories are not only correct but also logically sound and grounded in detailed visual evidence, teaching our model to perform nuanced visual reasoning.

A.3. Component 3: Augmenting with Text-Only Trajectories

Finally, to ensure our model can efficiently handle simpler questions where extensive visual re-examination is unnecessary, we augment the SFT dataset with purely textual reasoning trajectories. These “thinking about images” trajectories teach the model to answer questions when the visual information from the initial encoding is self-evident (Yang et al., 2025b). This component is sourced in two ways:

- For datasets that already provide text-only reasoning chains (Zhang et al., 2025d; Wang et al., 2025a), we use them directly.

Table 4. Statistics of the dataset for our two-stage (SFT+RL) training. The SFT stage utilizes two types of reasoning trajectories: standard textual-only and our proposed “Chatting with Images.” We either repurpose existing trajectories from source datasets (✓) or synthesize both types from scratch where none are provided (✗). MC: Multiple-Choice.

Source	Domain	Visual Input	Task Type	Trajectory Provided	SFT		RL
					Textual	Chatting with Images	
VGR (Wang et al., 2025c)	General	Single Image	MC	✓	0	30,090	8,629
Thyme (Zhang et al., 2025d)	General	Single Image	MC	✓	96,402	70,375	9,378
SpaceR (Ouyang et al., 2025)	Spatial Reasoning	Video	MC / Numerical	✗	11,629	25,973	19,316
SPAR (Zhang et al., 2025b)	Spatial Reasoning	Video	MC / Numerical	✗	9,280	26,607	13,779
Vica (Feng, 2025)	Spatial Reasoning	Video	MC / Numerical	✗	25,307	11,332	68,898

Prompt for “Thinking with Images” Data Conversion

You are a highly intelligent data extraction agent. Please analyze a conversation between a user and a tool- or code-using AI model, and convert it into a structured JSON format. Given the user instruction and model response below, extract a list where each element corresponds to one ‘<code>’ block or ‘bounding box’.

Field Definitions:

- **thought:** The high-level reasoning or planning text that precedes a code/box. It describes the model’s internal monologue, connecting previous observations to the motivation for the upcoming inquiry.
- **target_region:** A list specifying the target(s) of the inquiry. Each item in this list defines which image is used and where on that image the inquiry is applied.
 - **image_index:** Identifies the target image.
 - **bbox_2d:** A list of four integer coordinates ‘[x1, y1, x2, y2]’...
- **Inquiry:** This is the semantic goal of the code/box. It must describe the information the code/box is trying to highlight, verify, or expose within the specified ‘bbox_2d’. It is the ‘why’ behind the crop, not just the act of cropping.

Output Schema:

```
[
  {
    "thought": "The reasoning process leading to the target regions and inquiry",
    "target_region": [
      {
        "image_index": "The index of the first image...",
        "bbox_2d": [x1, y1, x2, y2]
      },
      ...
    ],
    "inquiry": "The inferred purpose of the corresponding code block or bounding box."
  },
  ...
]
```

Figure 6. The detailed prompt structure used to translate heterogeneous, tool- or code-based reasoning trajectories into a unified, structured JSON format for SFT.

- For datasets without such annotations, we use Qwen2.5-VL-72B to generate reasoning chains via rejection sampling (Dubey et al., 2024). We generate multiple candidate trajectories for each question and retain only those that lead to the correct final answer, ensuring the quality of the synthesized data.

This hybrid data strategy equips ViLAVT with the ability to dynamically choose between deep, iterative visual thinking and efficient, text-based reasoning, depending on the complexity of the query.

B. Benchmark Details

We conduct comprehensive evaluations across two categories of benchmarks, each targeting distinct capabilities of vision-language models.

High-Resolution Perception Benchmarks. These benchmarks assess a model’s ability to compress high-resolution visual information while maintaining fine-grained detail perception and conducting precise visual search—tasks that pose significant challenges to current VLMs. We employ *HRBench-4K* and *HRBench-8K* (Wang et al., 2025d), which evaluate model performance on 4K and 8K resolution images, respectively.

Spatial Reasoning Benchmarks. These benchmarks eval-

Table 5. Statistics of examples in high-resolution and spatial reasoning benchmarks.

High-Resolution		Spatial Reasoning						
Single-Image		Single-Image		Multi-view			Video	
HRBench-4K	HRBench-8K	SpatialEval-Real	EmbSpatial	ERQA	SPAR-Bench	MMSI-Bench	VSI-Bench	
800	800	135	3,640	400	7,211	1,000	5,130	

Table 6. Comparative per-round overhead analysis of different reasoning paradigms. For interactive methods, we report the average latency of a single reasoning–interaction round, since different paradigms may require varying numbers of rounds. Our paradigm achieves high flexibility with a controlled overhead.

Paradigm	Model Example	Relative Latency	Key Overhead Source
Static (Non Thinking)	Qwen2.5-VL	2.51s (-)	Single forward pass
Static (Thinking <i>about</i> Images)	Qwen2.5-VL	4.69s (1.0 \times)	Single forward pass
Tool-based (Thinking <i>with</i> Images)	ViLaSR (Wu et al., 2025b)	6.05s (1.28 \times)	External tool calls, I/O
Code-based (Thinking <i>with</i> Images)	Thyme (Zhang et al., 2025d)	6.18s (1.31 \times)	Code interpreter, process isolation, I/O
Ours (Chatting <i>with</i> Images)	VILAVT (Ours)	5.97s (1.06\times)	Internal feature re-computation

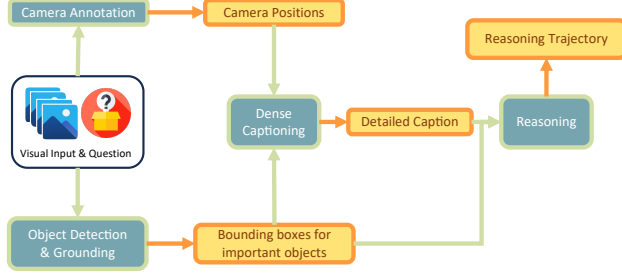


Figure 7. The dedicated pipeline for synthesizing high-quality spatial reasoning trajectories. We first mine latent knowledge (objects, grounding, camera motion, captions) and then use this rich context to guide a powerful teacher model (Qwen2.5-VL-72B) in generating a detailed reasoning path.

ate the model’s capacity to understand complex spatial and temporal relationships encoded in visual data. We organize them by input modality:

- **Single-image reasoning:** *SpatialEval-Real* (Wang et al., 2024) and *EmbSpatial* (Du et al., 2024) test spatial understanding within individual images.
- **Multi-image reasoning:** *ERQA* (Team et al., 2025), *SPAR-Bench* (Zhang et al., 2025b), and *MMSI-Bench* (Yang et al., 2025c) evaluate cross-image spatial reasoning.
- **Video-based reasoning:** *VSI-Bench* (Yang et al., 2024) assess spatiotemporal understanding in video sequences.

Table 5 summarizes the dataset statistics across all benchmarks.

C. Implementation Details

- **Vision encoder architecture.** The re-invented vision Transformer \mathcal{V}_e in VILAVT comprises 32 Transformer

layers with 16 attention heads and a hidden dimension of 1280, inherited from Qwen2.5-VL (Bai et al., 2025). The lightweight language Transformer \mathcal{V}_m is a frozen Qwen3-Embedding-0.6B model.³ We employ a hybrid attention mechanism across different layers:

- *Intra-full attention* (layers 8, 16): Attention is operated within individual images.
- *Inter-full attention* (layers 17–32): Full self-attention jointly operates over all visual tokens from multiple images and the textual inquiry, enabling query-conditioned cross-view interactions.
- *Sparse window attention* (remaining layers): attention is confined to local patch windows for efficiency.
- *Sparse window attention* (remaining layers): Attention is confined to local patch windows for computational efficiency.
- **SFT.** In the SFT stage, we train for 2 epochs with a global batch size of 384, using AdamW (Loshchilov & Hutter, 2019) with a learning rate of 5×10^{-5} .
- **RL.** The RL stage follows the VeRL framework (Sheng et al., 2024). For each instance, we generate $G = 4$ candidate trajectories per rollout. A rollout terminates when a final answer is produced, when the number of interaction rounds exceeds T_{\max} (5 for general tasks and 10 for spatial reasoning), or when a cumulative limit of 52 processed visual inputs is reached. The policy is updated with a batch size of 96, and $\epsilon_1/\epsilon_2/\delta$ in Eq. 6 are set to 0.2/0.3/10 $^{-6}$, respectively.
- **Hardware and training infrastructure.** All experi-

³<https://huggingface.co/Qwen/Qwen3-Embedding-0.6B>

Visual Input & QA	Source Reasoning Process	Target Reasoning Process
 <p>Question: What is the pose of the child?</p>	<p><think> To accurately determine the pose of the child in the image, it's essential to focus on the specific area where the child is located. Cropping and zooming in on this region will help eliminate distractions and provide a clearer view of the child's posture and actions. The goal of the task is to analyze the child's pose. To improve visibility, I will crop the region around the child and zoom in. Based on the provided visual information, the child is located near the center-right of the image, slightly below the balloons. I will refine this region to increase clarity and focus on the relevant portion of the image.</p> <pre data-bbox="396 523 543 593"><code> ``` python import cv2 import os import random # Load the image image_path = "/mlm_hdd/yfzhang/data/lava_sf/gqa/images/2387301.jpg" image = cv2.imread(image_path) # Define the initial bounding box for cropping (based on the reference visual information) x1, y1, x2, y2 = 157, 8, 292, 147 # Crop the image using the defined bounding box cropped_image = image[y1:y2, x1:x2] # Save the cropped image with a random suffix in a temporary directory temp_dir = os.path.join(tempfile.gettempdir(), "cropped_images") random_suffix = str(random.randint(1000, 9999)) filename = os.path.basename(image_path) processed_filename = f"{os.path.splitext(filename)[0]}_{random_suffix}{os.path.splitext(filename)[1]}" processed_path = os.path.join(temp_dir, processed_filename) cv2.imwrite(processed_path, cropped_image) # Print the path of the saved cropped image for further processing print(processed_path) ``` </code> <sandbox_output><image></sandbox_output></pre>	<p><think> To accurately determine the pose of the child in the image, it's essential to focus on the specific area where the child is located. Cropping and zooming in on this region will help eliminate distractions and provide a clearer view of the child's posture and actions. The goal of the task is to analyze the child's pose. To improve visibility, I will crop the region around the child and zoom in. Based on the provided visual information, the child is located near the center-right of the image, slightly below the balloons. I will refine this region to increase clarity and focus on the relevant portion of the image. </think></p> <p><tool> {"target_region": [{"index": 0, "bbox_2d": [158, 8, 294, 143]}], "inquiry": "Identify the child's location and improve visibility for pose analysis."} </tool></p>
<p>Answer: The pose of the child is standing.</p>	<p># Define the initial bounding box for cropping (based on the reference visual information)</p> <pre data-bbox="396 593 543 665">x1, y1, x2, y2 = 157, 8, 292, 147</pre> <p># Crop the image using the defined bounding box</p> <pre data-bbox="396 665 543 760">cropped_image = image[y1:y2, x1:x2]</pre> <p># Save the cropped image with a random suffix in a temporary directory</p> <pre data-bbox="396 760 543 806">temp_dir = os.path.join(tempfile.gettempdir(), "cropped_images") random_suffix = str(random.randint(1000, 9999)) filename = os.path.basename(image_path) processed_filename = f"{os.path.splitext(filename)[0]}_{random_suffix}{os.path.splitext(filename)[1]}" processed_path = os.path.join(temp_dir, processed_filename) cv2.imwrite(processed_path, cropped_image)</pre> <p># Print the path of the saved cropped image for further processing</p> <pre data-bbox="396 806 543 861">print(processed_path) ``` </code> <sandbox_output><image></sandbox_output></pre>	<p><think> Wait, it appears this crop does not target the desired object, which is the child. Upon reviewing the image again, it seems the child is positioned more towards the center-right of the image, closer to the table with food. Therefore, a new set of coordinates is required to crop and emphasize the child properly. Using the correct bounding box, I will now crop the image accurately to focus on the child. This will allow for a detailed analysis of the child's pose.</p>
<p>Wait, it appears this crop does not target the desired object, which is the child. Upon reviewing the image again, it seems the child is positioned more towards the center-right of the image, closer to the table with food. Therefore, a new set of coordinates is required to crop and emphasize the child properly. Using the correct bounding box, I will now crop the image accurately to focus on the child. This will allow for a detailed analysis of the child's pose.</p>	<p><code> ``` # Define the correct bounding box for cropping (based on the inferred visual information) x1, y1, x2, y2 = 268, 164, 321, 272 ``` </code> <sandbox_output><image></sandbox_output></p>	<p><think> After cropping the image correctly, the analysis of the child's pose reveals that the child is standing and appears to be observing or interacting with the food on the table. The child's body is slightly turned, and their arms are relaxed at their sides, indicating a casual and attentive stance. This pose suggests the child is engaged in the activity happening around the table, possibly waiting for their turn or observing others. </think></p> <p><answer> The pose of the child is standing. </answer></p>
<p>After cropping the image correctly, the analysis of the child's pose reveals that the child is standing and appears to be observing or interacting with the food on the table. The child's body is slightly turned, and their arms are relaxed at their sides, indicating a casual and attentive stance. This pose suggests the child is engaged in the activity happening around the table, possibly waiting for their turn or observing others. </think></p>	<p><code> ``` # Define the correct bounding box for cropping (based on the inferred visual information) x1, y1, x2, y2 = 268, 164, 321, 272 ``` </code> <sandbox_output><image></sandbox_output></p>	<p><think> The question asks if this is a fitness book. Analyzing the image, the title "The Legend of the African Baobab Tree" suggests it is about the legend and nature of the baobab tree, not fitness-related topics. The illustration shows baobab tree and African wildlife. <box>[0,95,386,495]</box>, which is typical of children's or nature-related books, not fitness books. Fitness books usually feature elements like people exercising, fitness equipment, or health and diet tips, which are absent here. So, based on the title and illustration, it is not a fitness book. </think></p> <p><answer>No</answer></p>
<p><think> The question asks if this is a fitness book. Analyzing the image, the title "The Legend of the African Baobab Tree" suggests it is about the legend and nature of the baobab tree, not fitness-related topics. The illustration shows baobab tree and African wildlife. <box>[0,95,386,495]</box>, which is typical of children's or nature-related books, not fitness books. Fitness books usually feature elements like people exercising, fitness equipment, or health and diet tips, which are absent here. So, based on the title and illustration, it is not a fitness book. </think></p>	<p><code> ``` # Define the correct bounding box for cropping (based on the inferred visual information) x1, y1, x2, y2 = 268, 164, 321, 272 ``` </code> <sandbox_output><image></sandbox_output></p>	<p><think> The question asks if this is a fitness book. To determine the book's category, I need to examine the title for clues about its content. </think></p>
<p><answer> No </answer></p>	<p><code> ``` # Define the correct bounding box for cropping (based on the inferred visual information) x1, y1, x2, y2 = 268, 164, 321, 272 ``` </code> <sandbox_output><image></sandbox_output></p>	<p><tool> {"target_region": [{"index": 0, "bbox_2d": [0, 0, 392, 136]}], "inquiry": "Identify the title of the book to understand its subject matter."} </tool></p>
<p>After examining the title and illustration, the book is identified as "The Legend of the African Baobab Tree". The title suggests the book is about the legend and nature of the baobab tree, not fitness-related topics. The illustration shows a baobab tree and African wildlife, which is typical of children's or nature-related books, not fitness books. Fitness books usually feature elements like people exercising, fitness equipment, or health and diet tips, which are absent here. So, based on the title and illustration, it is not a fitness book. </think></p>	<p><code> ``` # Define the correct bounding box for cropping (based on the inferred visual information) x1, y1, x2, y2 = 268, 164, 321, 272 ``` </code> <sandbox_output><image></sandbox_output></p>	<p><think> The title is "The Legend of the African Baobab Tree". The title suggests the book is about the legend and nature of the baobab tree, not fitness-related topics. Next, I should examine the illustration for further context. To further confirm the book's category, I need to analyze the illustration for any fitness-related elements. </think></p>
<p><answer> No </answer></p>	<p><code> ``` # Define the correct bounding box for cropping (based on the inferred visual information) x1, y1, x2, y2 = 268, 164, 321, 272 ``` </code> <sandbox_output><image></sandbox_output></p>	<p><tool> {"target_region": [{"index": 0, "bbox_2d": [0, 95, 386, 495]}], "inquiry": "Examine the illustration for any elements that might indicate the book's subject matter."} </tool></p>
<p><think> The illustration shows a baobab tree and African wildlife. The illustration shows a baobab tree and African wildlife, which is typical of children's or nature-related books, not fitness books. Fitness books usually feature elements like people exercising, fitness equipment, or health and diet tips, which are absent here. So, based on the title and illustration, it is not a fitness book. Based on the analysis of the title and illustration, I can conclude whether the book is related to fitness. </think></p>	<p><code> ``` # Define the correct bounding box for cropping (based on the inferred visual information) x1, y1, x2, y2 = 268, 164, 321, 272 ``` </code> <sandbox_output><image></sandbox_output></p>	<p><think> The illustration shows a baobab tree and African wildlife. The illustration shows a baobab tree and African wildlife, which is typical of children's or nature-related books, not fitness books. Fitness books usually feature elements like people exercising, fitness equipment, or health and diet tips, which are absent here. So, based on the title and illustration, it is not a fitness book. Based on the analysis of the title and illustration, I can conclude whether the book is related to fitness. </think></p> <p><answer> No </answer></p>

Figure 8. Illustration of our data unification process for SFT. This figure showcases how we convert heterogeneous, externally-interactive reasoning trajectories from existing datasets into our native “Chatting with Images” format. For each step in the Source Reasoning Process that involves an external action (in light green), we prompt a teacher model to translate it into our internal action format (in light orange). This target format consists of a natural language inquiry that captures the intent of the original action, and the corresponding target_region data. **Top Example** demonstrates the conversion of a complex, multi-step Python sandbox session. Note how the process handles a self-correction loop (the first crop is incorrect, leading to a second, refined action), translating procedural code execution into a sequence of declarative, language-guided inquiries. **Bottom Example** shows the same process applied to a simpler, tag-based tool, demonstrating the versatility of our unification strategy across different source formats. The highlighted sections in the Target Reasoning Process denote the generated `<tool>` calls, which form the core training signal for our model.

ments are conducted on a cluster of 96 NVIDIA H20 (80GB) GPUs. The SFT stage requires approximately 27 hours, while the RL stage takes roughly 138 hours under this configuration.

- **Inference optimization.** During evaluation and RL rollouts, we leverage vLLM (Kwon et al., 2023) for batched inference with optimized memory management. We use top- p sampling (Holtzman et al., 2020) ($p = 0.9$) with temperature 0.75 to generate reasoning trajectories and final answers. We adapt ViLAVT to the vLLM framework and will open-source our implementation upon paper acceptance.
- **Evaluation protocol.** We impose task-specific limits on tool usage: up to 10 tool calls for spatial reasoning tasks and 5 calls for high-resolution tasks. All high-resolution benchmarks are evaluated using VLMEvalKit (Duan et al., 2024) to ensure consistency with baseline methods. Final answers are extracted from `<answer>` tags and normalized before comparison.

D. More Analysis

D.1. Analysis of Training Dynamics

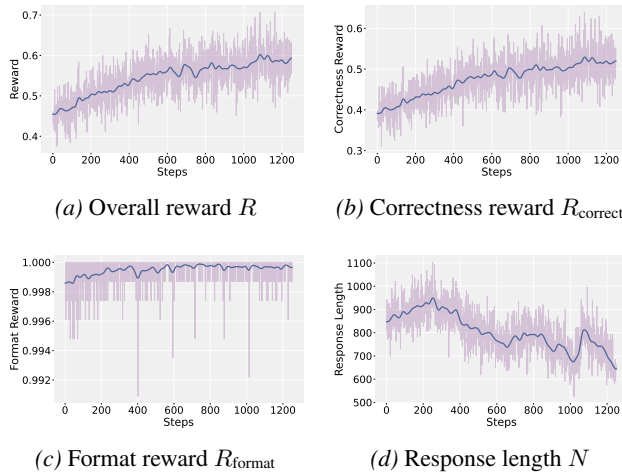


Figure 9. RL training dynamics of ViLAVT

Figure 9 illustrates the training dynamics of ViLAVT. We observe that both the correctness reward R_{correct} and the overall reward R exhibit a stable upward trend, indicating continuous optimization throughout training. The format reward R_{format} starts relatively high due to extensive supervised fine-tuning, which endows the model with strong format-following capabilities; it steadily approaches 1.0 as training progresses. It is noteworthy that the response length N increases over the first 200 training steps, peaks, and then gradually declines. We hypothesize that this reflects the

emergence of novel reasoning patterns in ViLAVT that differ from those present in the supervised data. In later RL iterations, N shows a decreasing trend but with noticeable fluctuations.

D.2. Overhead Analysis

Our “chatting with images” paradigm intentionally trades a controlled computational overhead for substantial gains in reasoning accuracy. We analyze this trade-off in Table 6, comparing our model’s per-round inference-stage overhead against both “thinking about image” and “thinking with image” paradigms on *HRBench-4K*. Since different interactive paradigms may require varying numbers of reasoning rounds, total inference time is not directly comparable; instead, we report the average cost of a single reasoning–interaction step. All timing measurements are recorded using standard Transformer inference without acceleration techniques.

As the analysis shows, while interactive reasoning is inherently more costly than a single-pass baseline, our per-round cost is comparable to, and slightly lower than, tool-based and code-based approaches. This efficiency stems from using a simple image crop operation and a unified manipulation interface via inquiry-conditioned, multi-image re-encoding, avoiding external tool I/O and code execution loops. In addition, (i) the inquiry encoder \mathcal{V}_m is a small frozen model with negligible overhead, and (ii) re-computation is applied only to cropped regions rather than the full-resolution input. Together, these choices yield a modest per-step overhead while remaining competitive with prior interactive paradigms.

D.3. Detailed results on VSI-Bench

In this section, we present detailed results of ViLAVT on *VSI-Bench* (Yang et al., 2024), a challenging benchmark covering eight diverse spatial reasoning tasks. Table 7 compares our method with state-of-the-art models across both numerical questions (object count, absolute distance, object size, room size) and multiple-choice questions (relative distance, relative direction, route planning, appearance order). The results highlight the comprehensive spatial reasoning capabilities of our approach.

E. Case Study

E.1. Representative Cases

Figure 10 demonstrates our paradigm’s strength on video-based spatial reasoning.

There are also three HRBench-4K cases that together highlight the strengths and weaknesses of different models in high-resolution visual perception and reasoning. In Fig-

ure 11, ViLAVT leverages a coarse-to-fine strategy—first scanning the full image, then cropping and zooming into small regions—to correctly identify that the person’s clothing is blue, whereas Thyme gives an incorrect cropping region. In Figure 12, ViLAVT again benefits from targeted cropping to correctly recognize the building’s red and white striped antenna, while GPT-5 directly outputs an incorrect answer and Thyme provides an answer without an explicit reasoning chain. In contrast, the example in Figure 13 shows that when the task mainly involves reasoning about relative spatial relationships, all three models can arrive at the correct answer, with ViLAVT explicitly grounding entities in the image and the others relying primarily on text-based reasoning.

E.2. Attention Map Visualization Cases

We extract attention maps from the last layer of the vision encoder, average them across all heads, and aggregate patch-level attention to form a single heatmap, which is overlaid on the original image for visualization.

We provide another attention map visualization case in Figure 14. Compared with ViLAVT w/o Inquiry and Qwen2.5-VL-7B with the vanilla ViT backbone, the query-aware vision encoder of ViLAVT focuses more strongly on the query-relevant object—the label in the red circle. This indicates that incorporating the textual query into the vision encoder facilitates more fine-grained detail extraction.

F. Prompt Template

The prompting framework of ViLAVT comprises a system prompt that encodes reasoning principles (Figure 15) and a user prompt template that structures visual inputs and tool interactions (Figure 16).



Measuring from the closest point of each object, which of these objects (tv, sofa, fireplace, chair) is the closest to the stove? Answer with the option's letter from the given choices directly.
 A. tv
 B. sofa
 C. fireplace
 D. chair

GPT-5 (thinking about images): Okay, let's analyze the image. From the provided images, the fireplace is located closest to the stove. Therefore, the answer is C. X

ViLaVT (chatting with images):

<think> To determine the location of the stove, we need to identify the image that shows the kitchen area. Image 19 clearly shows the kitchen. <think> <tool> {"region": [{"index": 19, "bbox_2d": [188, 309, 317, 437]}], "inquiry": "Where is the stove located?"} </tool>



<think> To determine the locations of the TV, sofa, fireplace, and chair, we need to identify the images that show these objects. Image 5 shows the living room with the TV, sofa, and fireplace. Image 27 shows the sofa with pillows. Image 26 shows the fireplace. Image 25 shows the chair near the door. <think> <tool> {"region": [{"index": 5, "bbox_2d": [0, 364, 504]}, {"index": 27, "bbox_2d": [33, 103, 250, 420]}, {"index": 26, "bbox_2d": [220, 172, 364, 368]}, {"index": 25, "bbox_2d": [0, 0, 209, 480]}], "inquiry": "Where are the TV, sofa, fireplace, and chair located?"} </tool>



<think> To determine which object is closest to the stove, we need to compare the distances between the stove and the TV, sofa, fireplace, and chair. The stove is in the kitchen (Image 19), and the TV, sofa, and fireplace are in the living room (Image 5, 26, 27). The living room and kitchen are separate rooms, so the closest object to the stove must be within the kitchen. We can see the chair directly against the kitchen island (Image 5, 25). Therefore, the chair is the closest object to the stove. </think> <answer> D </answer> ✓

Figure 10. A comparison on a multi-frame spatial reasoning task from VSI-Bench.

Table 7. Detailed Results on VSI-Bench.

Method	Sub-tasks								Average	
	Numerical questions				Multiple-choice questions					
	Object Count	Absolute Distance	Object Size	Room Size	Relative Distance	Relative Direction	Route Plan	Appearance Order		
Proprietary LVLMs										
GPT-4o	46.2	5.3	43.8	38.2	37.0	41.3	31.5	28.5	34.0	
Gemini-1.5-Flash	49.8	30.8	53.5	54.4	37.7	41.0	31.5	37.8	42.1	
Gemini-1.5-Pro	56.2	30.9	64.1	43.6	51.3	46.3	36.0	34.6	45.4	
Open-source LVLMs										
Qwen2.5-VL-7B	29.3	26.8	54.6	35.5	41.0	34.4	26.8	29.3	34.7	
Qwen2.5-VL-72B	33.9	27.2	59.3	28.5	47.2	35.3	22.2	34.5	36.0	
LLaVA-NeXT-Video-7B	48.5	14.0	47.8	24.2	43.5	42.4	34.0	30.6	35.6	
LLaVA-OneVision-7B	47.7	20.2	47.4	12.3	42.5	35.2	29.4	24.4	32.4	
Kimi-VL-A3B-Instruct-16B	-	-	-	-	-	-	-	-	37.4	
LLaVA-NeXT-Video-72B	48.9	22.8	57.4	35.3	42.4	36.7	35.0	48.6	40.9	
LLaVA-OneVision-72B	43.5	23.9	57.6	37.5	42.5	39.9	32.5	44.6	40.2	
InterVL2-8B	31.3	29.0	48.9	44.2	38.0	33.4	28.9	46.4	37.5	
Representative methods for spatial reasoning										
SpaceR-7B	62.3	31.8	60.5	40.2	42.1	46.8	32.0	48.2	45.5	
Spatial-MLLM-4B	65.3	34.8	63.1	45.1	41.3	46.2	33.5	46.3	48.4	
ViLaSR-7B	63.5	34.4	60.6	30.9	48.9	45.2	30.4	49.2	45.4	
Ours										
ViLaVT-SFT	35.9	32.8	61.4	39.8	43.7	42.2	29.9	60.7	43.3	
ViLaVT	65.8	39.0	69.2	55.5	50.8	46.0	23.7	66.3	52.0	



What's the primary color of the person's clothing in the image? A. Green B. Yellow. C. Blue D. White

GPT-5 (thinking about images): I first look for any person in the image, since the question asks about the color of their clothing. The scene shows terraced fields, mountains, and a small structure, but there is no clearly visible person whose clothing color can be identified. Therefore, I cannot reliably determine the primary color of a person's clothing from this image. Final answer: None of the options can be determined from the image. X

THYME (Code-based Thinking with Image):

<think> To determine the primary color of the person's clothing in the image, we need to focus on the individual located near the small structure in the middle-left portion of the image. The person appears quite small relative to the entire scene, so zooming in on this specific area is essential for accurately identifying the color of their clothing. Cropping and zooming in will help isolate the person and provide a clearer view of their clothing details.

The person is positioned near the structure, and zooming in on this area will allow us to observe the clothing color more closely. The coordinates for this region appear to be around the middle-left section of the image, slightly above the lower half. Cropping this area will help us focus on the person's clothing and determine the primary color.

Here is the Python code to crop and zoom in on the relevant area:

```
<code>
```
python
import os
import random
from PIL import Image

Load the image
image_path = "HRBench4K/168.jpg"
image = Image.open(image_path)

Define the coordinates for the region of interest (ROI)
The person is near the small structure in the middle-left part of the image
x1, y1, x2, y2 = 600, 1300, 750, 1400 # Adjust these coordinates based on the person's location

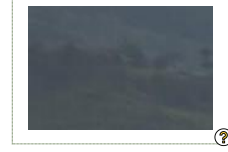
Crop the image based on the ROI
cropped_image = image.crop((x1, y1, x2, y2))

Save the cropped image with a random suffix in the temporary folder
temp_folder = "/mnt/data/temp_processed_images"
random_suffix = random.randint(1000, 9999)
filename = os.path.basename(image_path)
processed_filename = f"{os.path.splitext(filename)[0]}_{random_suffix}{os.path.splitext(filename)[1]}"
processed_path = os.path.join(temp_folder, processed_filename)
cropped_image.save(processed_path)

Print the path of the saved cropped image
print(processed_path)
```
</code>
<sandbox_output></sandbox_output>
```

Upon examining the cropped image, it is evident that the person's clothing is blue. The zoomed-in view allows us to clearly see the color, confirming that option C is correct. </think>

<answer> C </answer> ✓



VILAVT (chatting with images):

<think> The task involves identifying the primary color of the person's clothing in the image. The person appears to be quite small and located at a distance in the image, making it challenging to discern the exact color of their clothing. To accurately determine the color, it is necessary to zoom in on the specific region where the person is located. This will help in enhancing the details and making the color more distinguishable. To achieve this, I will crop the image around the area where the person is standing and apply a zoom to improve the visibility of the clothing color. The coordinates for this region appear to be near the center-left of the image, slightly above the middle. I'll refine this area further for better clarity. </think> <tool> {"region": [{"index": 0, "bbox_2d": [550, 120, 600, 180]}, {"index": 1, "bbox_2d": [550, 180, 600, 240]}, {"index": 2, "bbox_2d": [550, 240, 600, 300]}, {"index": 3, "bbox_2d": [550, 300, 600, 360]}, {"index": 4, "bbox_2d": [550, 360, 600, 420]}, {"index": 5, "bbox_2d": [550, 420, 600, 480]}, {"index": 6, "bbox_2d": [550, 480, 600, 540]}, {"index": 7, "bbox_2d": [550, 540, 600, 600]}, {"index": 8, "bbox_2d": [550, 600, 600, 660]}, {"index": 9, "bbox_2d": [550, 660, 600, 720]}, {"index": 10, "bbox_2d": [550, 720, 600, 780]}, {"index": 11, "bbox_2d": [550, 780, 600, 840]}, {"index": 12, "bbox_2d": [550, 840, 600, 900]}, {"index": 13, "bbox_2d": [550, 900, 600, 960]}, {"index": 14, "bbox_2d": [600, 120, 650, 180]}, {"index": 15, "bbox_2d": [600, 180, 650, 240]}, {"index": 16, "bbox_2d": [600, 240, 650, 300]}, {"index": 17, "bbox_2d": [600, 300, 650, 360]}, {"index": 18, "bbox_2d": [600, 360, 650, 420]}, {"index": 19, "bbox_2d": [600, 420, 650, 480]}, {"index": 20, "bbox_2d": [600, 480, 650, 540]}, {"index": 21, "bbox_2d": [600, 540, 650, 600]}, {"index": 22, "bbox_2d": [600, 600, 650, 660]}, {"index": 23, "bbox_2d": [600, 660, 650, 720]}, {"index": 24, "bbox_2d": [600, 720, 650, 780]}, {"index": 25, "bbox_2d": [600, 780, 650, 840]}, {"index": 26, "bbox_2d": [600, 840, 650, 900]}, {"index": 27, "bbox_2d": [600, 900, 650, 960]}, {"index": 28, "bbox_2d": [650, 120, 700, 180]}, {"index": 29, "bbox_2d": [650, 180, 700, 240]}, {"index": 30, "bbox_2d": [650, 240, 700, 300]}, {"index": 31, "bbox_2d": [650, 300, 700, 360]}, {"index": 32, "bbox_2d": [650, 360, 700, 420]}, {"index": 33, "bbox_2d": [650, 420, 700, 480]}, {"index": 34, "bbox_2d": [650, 480, 700, 540]}, {"index": 35, "bbox_2d": [650, 540, 700, 600]}, {"index": 36, "bbox_2d": [650, 600, 700, 660]}, {"index": 37, "bbox_2d": [650, 660, 700, 720]}, {"index": 38, "bbox_2d": [650, 720, 700, 780]}, {"index": 39, "bbox_2d": [650, 780, 700, 840]}, {"index": 40, "bbox_2d": [650, 840, 700, 900]}, {"index": 41, "bbox_2d": [700, 780, 750, 840]}, {"index": 42, "bbox_2d": [700, 840, 750, 900]}, {"index": 43, "bbox_2d": [750, 780, 800, 840]}, {"index": 44, "bbox_2d": [750, 840, 800, 900]}, {"index": 45, "bbox_2d": [800, 780, 850, 840]}, {"index": 46, "bbox_2d": [800, 840, 850, 900]}, {"index": 47, "bbox_2d": [850, 780, 900, 840]}, {"index": 48, "bbox_2d": [850, 840, 900, 900]}, {"index": 49, "bbox_2d": [900, 780, 950, 840]}, {"index": 50, "bbox_2d": [900, 840, 950, 900]}, {"index": 51, "bbox_2d": [950, 780, 1000, 840]}, {"index": 52, "bbox_2d": [950, 840, 1000, 900]}, {"index": 53, "bbox_2d": [1000, 780, 1050, 840]}, {"index": 54, "bbox_2d": [1000, 840, 1050, 900]}, {"index": 55, "bbox_2d": [1050, 780, 1100, 840]}, {"index": 56, "bbox_2d": [1050, 840, 1100, 900]}, {"index": 57, "bbox_2d": [1100, 780, 1150, 840]}, {"index": 58, "bbox_2d": [1100, 840, 1150, 900]}, {"index": 59, "bbox_2d": [1150, 780, 1200, 840]}, {"index": 60, "bbox_2d": [1150, 840, 1200, 900]}, {"index": 61, "bbox_2d": [1200, 780, 1250, 840]}, {"index": 62, "bbox_2d": [1200, 840, 1250, 900]}, {"index": 63, "bbox_2d": [1250, 780, 1300, 840]}, {"index": 64, "bbox_2d": [1250, 840, 1300, 900]}, {"index": 65, "bbox_2d": [1300, 780, 1350, 840]}, {"index": 66, "bbox_2d": [1300, 840, 1350, 900]}, {"index": 67, "bbox_2d": [1350, 780, 1400, 840]}, {"index": 68, "bbox_2d": [1350, 840, 1400, 900]}, {"index": 69, "bbox_2d": [1400, 780, 1450, 840]}, {"index": 70, "bbox_2d": [1400, 840, 1450, 900]}, {"index": 71, "bbox_2d": [1450, 780, 1500, 840]}, {"index": 72, "bbox_2d": [1450, 840, 1500, 900]}, {"index": 73, "bbox_2d": [1500, 780, 1550, 840]}, {"index": 74, "bbox_2d": [1500, 840, 1550, 900]}, {"index": 75, "bbox_2d": [1550, 780, 1600, 840]}, {"index": 76, "bbox_2d": [1550, 840, 1600, 900]}, {"index": 77, "bbox_2d": [1600, 780, 1650, 840]}, {"index": 78, "bbox_2d": [1600, 840, 1650, 900]}, {"index": 79, "bbox_2d": [1650, 780, 1700, 840]}, {"index": 80, "bbox_2d": [1650, 840, 1700, 900]}, {"index": 81, "bbox_2d": [1700, 780, 1750, 840]}, {"index": 82, "bbox_2d": [1700, 840, 1750, 900]}, {"index": 83, "bbox_2d": [1750, 780, 1800, 840]}, {"index": 84, "bbox_2d": [1750, 840, 1800, 900]}, {"index": 85, "bbox_2d": [1800, 780, 1850, 840]}, {"index": 86, "bbox_2d": [1800, 840, 1850, 900]}, {"index": 87, "bbox_2d": [1850, 780, 1900, 840]}, {"index": 88, "bbox_2d": [1850, 840, 1900, 900]}, {"index": 89, "bbox_2d": [1900, 780, 1950, 840]}, {"index": 90, "bbox_2d": [1900, 840, 1950, 900]}, {"index": 91, "bbox_2d": [1950, 780, 2000, 840]}, {"index": 92, "bbox_2d": [1950, 840, 2000, 900]}, {"index": 93, "bbox_2d": [2000, 780, 2050, 840]}, {"index": 94, "bbox_2d": [2000, 840, 2050, 900]}, {"index": 95, "bbox_2d": [2050, 780, 2100, 840]}, {"index": 96, "bbox_2d": [2050, 840, 2100, 900]}, {"index": 97, "bbox_2d": [2100, 780, 2150, 840]}, {"index": 98, "bbox_2d": [2100, 840, 2150, 900]}, {"index": 99, "bbox_2d": [2150, 780, 2200, 840]}, {"index": 100, "bbox_2d": [2150, 840, 2200, 900]}, {"index": 101, "bbox_2d": [2200, 780, 2250, 840]}, {"index": 102, "bbox_2d": [2200, 840, 2250, 900]}, {"index": 103, "bbox_2d": [2250, 780, 2300, 840]}, {"index": 104, "bbox_2d": [2250, 840, 2300, 900]}, {"index": 105, "bbox_2d": [2300, 780, 2350, 840]}, {"index": 106, "bbox_2d": [2300, 840, 2350, 900]}, {"index": 107, "bbox_2d": [2350, 780, 2400, 840]}, {"index": 108, "bbox_2d": [2350, 840, 2400, 900]}, {"index": 109, "bbox_2d": [2400, 780, 2450, 840]}, {"index": 110, "bbox_2d": [2400, 840, 2450, 900]}, {"index": 111, "bbox_2d": [2450, 780, 2500, 840]}, {"index": 112, "bbox_2d": [2450, 840, 2500, 900]}, {"index": 113, "bbox_2d": [2500, 780, 2550, 840]}, {"index": 114, "bbox_2d": [2500, 840, 2550, 900]}, {"index": 115, "bbox_2d": [2550, 780, 2600, 840]}, {"index": 116, "bbox_2d": [2550, 840, 2600, 900]}, {"index": 117, "bbox_2d": [2600, 780, 2650, 840]}, {"index": 118, "bbox_2d": [2600, 840, 2650, 900]}, {"index": 119, "bbox_2d": [2650, 780, 2700, 840]}, {"index": 120, "bbox_2d": [2650, 840, 2700, 900]}, {"index": 121, "bbox_2d": [2700, 780, 2750, 840]}, {"index": 122, "bbox_2d": [2700, 840, 2750, 900]}, {"index": 123, "bbox_2d": [2750, 780, 2800, 840]}, {"index": 124, "bbox_2d": [2750, 840, 2800, 900]}, {"index": 125, "bbox_2d": [2800, 780, 2850, 840]}, {"index": 126, "bbox_2d": [2800, 840, 2850, 900]}, {"index": 127, "bbox_2d": [2850, 780, 2900, 840]}, {"index": 128, "bbox_2d": [2850, 840, 2900, 900]}, {"index": 129, "bbox_2d": [2900, 780, 2950, 840]}, {"index": 130, "bbox_2d": [2900, 840, 2950, 900]}, {"index": 131, "bbox_2d": [2950, 780, 3000, 840]}, {"index": 132, "bbox_2d": [2950, 840, 3000, 900]}, {"index": 133, "bbox_2d": [3000, 780, 3050, 840]}, {"index": 134, "bbox_2d": [3000, 840, 3050, 900]}, {"index": 135, "bbox_2d": [3050, 780, 3100, 840]}, {"index": 136, "bbox_2d": [3050, 840, 3100, 900]}, {"index": 137, "bbox_2d": [3100, 780, 3150, 840]}, {"index": 138, "bbox_2d": [3100, 840, 3150, 900]}, {"index": 139, "bbox_2d": [3150, 780, 3200, 840]}, {"index": 140, "bbox_2d": [3150, 840, 3200, 900]}, {"index": 141, "bbox_2d": [3200, 780, 3250, 840]}, {"index": 142, "bbox_2d": [3200, 840, 3250, 900]}, {"index": 143, "bbox_2d": [3250, 780, 3300, 840]}, {"index": 144, "bbox_2d": [3250, 840, 3300, 900]}, {"index": 145, "bbox_2d": [3300, 780, 3350, 840]}, {"index": 146, "bbox_2d": [3300, 840, 3350, 900]}, {"index": 147, "bbox_2d": [3350, 780, 3400, 840]}, {"index": 148, "bbox_2d": [3350, 840, 3400, 900]}, {"index": 149, "bbox_2d": [3400, 780, 3450, 840]}, {"index": 150, "bbox_2d": [3400, 840, 3450, 900]}, {"index": 151, "bbox_2d": [3450, 780, 3500, 840]}, {"index": 152, "bbox_2d": [3450, 840, 3500, 900]}, {"index": 153, "bbox_2d": [3500, 780, 3550, 840]}, {"index": 154, "bbox_2d": [3500, 840, 3550, 900]}, {"index": 155, "bbox_2d": [3550, 780, 3600, 840]}, {"index": 156, "bbox_2d": [3550, 840, 3600, 900]}, {"index": 157, "bbox_2d": [3600, 780, 3650, 840]}, {"index": 158, "bbox_2d": [3600, 840, 3650, 900]}, {"index": 159, "bbox_2d": [3650, 780, 3700, 840]}, {"index": 160, "bbox_2d": [3650, 840, 3700, 900]}, {"index": 161, "bbox_2d": [3700, 780, 3750, 840]}, {"index": 162, "bbox_2d": [3700, 840, 3750, 900]}, {"index": 163, "bbox_2d": [3750, 780, 3800, 840]}, {"index": 164, "bbox_2d": [3750, 840, 3800, 900]}, {"index": 165, "bbox_2d": [3800, 780, 3850, 840]}, {"index": 166, "bbox_2d": [3800, 840, 3850, 900]}, {"index": 167, "bbox_2d": [3850, 780, 3900, 840]}, {"index": 168, "bbox_2d": [3850, 840, 3900, 900]}, {"index": 169, "bbox_2d": [3900, 780, 3950, 840]}, {"index": 170, "bbox_2d": [3900, 840, 3950, 900]}, {"index": 171, "bbox_2d": [3950, 780, 4000, 840]}, {"index": 172, "bbox_2d": [3950, 840, 4000, 900]}, {"index": 173, "bbox_2d": [4000, 780, 4050, 840]}, {"index": 174, "bbox_2d": [4000, 840, 4050, 900]}, {"index": 175, "bbox_2d": [4050, 780, 4100, 840]}, {"index": 176, "bbox_2d": [4050, 840, 4100, 900]}, {"index": 177, "bbox_2d": [4100, 780, 4150, 840]}, {"index": 178, "bbox_2d": [4100, 840, 4150, 900]}, {"index": 179, "bbox_2d": [4150, 780, 4200, 840]}, {"index": 180, "bbox_2d": [4150, 840, 4200, 900]}, {"index": 181, "bbox_2d": [4200, 780, 4250, 840]}, {"index": 182, "bbox_2d": [4200, 840, 4250, 900]}, {"index": 183, "bbox_2d": [4250, 780, 4300, 840]}, {"index": 184, "bbox_2d": [4250, 840, 4300, 900]}, {"index": 185, "bbox_2d": [4300, 780, 4350, 840]}, {"index": 186, "bbox_2d": [4300, 840, 4350, 900]}, {"index": 187, "bbox_2d": [4350, 780, 4400, 840]}, {"index": 188, "bbox_2d": [4350, 840, 4400, 900]}, {"index": 189, "bbox_2d": [4400, 780, 4450, 840]}, {"index": 190, "bbox_2d": [4400, 840, 4450, 900]}, {"index": 191, "bbox_2d": [4450, 780, 4500, 840]}, {"index": 192, "bbox_2d": [4450, 840, 4500, 900]}, {"index": 193, "bbox_2d": [4500, 780, 4550, 840]}, {"index": 194, "bbox_2d": [4500, 840, 4550, 900]}, {"index": 195, "bbox_2d": [4550, 780, 4600, 840]}, {"index": 196, "bbox_2d": [4550, 840, 4600, 900]}, {"index": 197, "bbox_2d": [4600, 780, 4650, 840]}, {"index": 198, "bbox_2d": [4600, 840, 4650, 900]}, {"index": 199, "bbox_2d": [4650, 780, 4700, 840]}, {"index": 200, "bbox_2d": [4650, 840, 4700, 900]}, {"index": 201, "bbox_2d": [4700, 780, 4750, 840]}, {"index": 202, "bbox_2d": [4700, 840, 4750, 900]}, {"index": 203, "bbox_2d": [4750, 780, 4800, 840]}, {"index": 204, "bbox_2d": [4750, 840, 4800, 900]}, {"index": 205, "bbox_2d": [4800, 780, 4850, 840]}, {"index": 206, "bbox_2d": [4800, 840, 4850, 900]}, {"index": 207, "bbox_2d": [4850, 780, 4900, 840]}, {"index": 208, "bbox_2d": [4850, 840, 4900, 900]}, {"index": 209, "bbox_2d": [4900, 780, 4950, 840]}, {"index": 210, "bbox_2d": [4900, 840, 4950, 900]}, {"index": 211, "bbox_2d": [4950, 780, 5000, 840]}, {"index": 212, "bbox_2d": [4950, 840, 5000, 900]}, {"index": 213, "bbox_2d": [5000, 780, 5050, 840]}, {"index": 214, "bbox_2d": [5000, 840, 5050, 900]}, {"index": 215, "bbox_2d": [5050, 780, 5100, 840]}, {"index": 216, "bbox_2d": [5050, 840, 5100, 900]}, {"index": 217, "bbox_2d": [5100, 780, 5150, 840]}, {"index": 218, "bbox_2d": [5100, 840, 5150, 900]}, {"index": 219, "bbox_2d": [5150, 780, 5200, 840]}, {"index": 220, "bbox_2d": [5150, 840, 5200, 900]}, {"index": 221, "bbox_2d": [5200, 780, 5250, 840]}, {"index": 222, "bbox_2d": [5200, 840, 5250, 900]}, {"index": 223, "bbox_2d": [5250, 780, 5300, 840]}, {"index": 224, "bbox_2d": [5250, 840, 5300, 900]}, {"index": 225, "bbox_2d": [5300, 780, 5350, 840]}, {"index": 226, "bbox_2d": [5300, 840, 5350, 900]}, {"index": 227, "bbox_2d": [5350, 780, 5400, 840]}, {"index": 228, "bbox_2d": [5350, 840, 5400, 900]}, {"index": 229, "bbox_2d": [5400, 780, 5450, 840]}, {"index": 230, "bbox_2d": [5400, 840, 5450, 900]}, {"index": 231, "bbox_2d": [5450, 780, 5500, 840]}, {"index": 232, "bbox_2d": [5450, 840, 5500, 900]}, {"index": 233, "bbox_2d": [5500, 780, 5550, 840]}, {"index": 234, "bbox_2d": [5500, 840, 5550, 900]}, {"index": 235, "bbox_2d": [5550, 780, 5600, 840]}, {"index": 236, "bbox_2d": [5550, 840, 5600, 900]}, {"index": 237, "bbox_2d": [5600, 780, 5650, 840]}, {"index": 238, "bbox_2d": [5600, 840, 5650, 900]}, {"index": 239, "bbox_2d": [5650, 780, 5700, 840]}, {"index": 240, "bbox_2d": [5650, 840, 5700, 900]}, {"index": 241, "bbox_2d": [5700, 780, 5750, 840]}, {"index": 242, "bbox_2d": [5700, 840, 5750, 900]}, {"index": 243, "bbox_2d": [5750, 780, 5800, 840]}, {"index": 244, "bbox_2d": [5750, 840, 5800, 900]}, {"index": 245, "bbox_2d": [5800, 780, 5850, 840]}, {"index": 246, "bbox_2d": [5800, 840, 5850, 900]}, {"index": 247, "bbox_2d": [5850, 780, 5900, 840]}, {"index": 248, "bbox_2d": [5850, 840, 5900, 900]}, {"index": 249, "bbox_2d": [5900, 780, 5950, 840]}, {"index": 250, "bbox_2d": [5900, 840, 5950, 900]}, {"index": 251, "bbox_2d": [5950, 780, 6000, 840]}, {"index": 252, "bbox_2d": [5950, 840, 6000, 900]}, {"index": 253, "bbox_2d": [6000, 780, 6050, 840]}, {"index": 254, "bbox_2d": [6000, 840, 6050, 900]}, {"index": 255, "bbox_2d": [6050, 780, 6100, 840]}, {"index": 256, "bbox_2d": [6050, 840, 6100, 900]}, {"index": 257, "bbox_2d": [6100, 780, 6150, 840]}, {"index": 258, "bbox_2d": [6100, 840, 6150, 900]}, {"index": 259, "bbox_2d": [6150, 780, 6200, 840]}, {"index": 260, "bbox_2d": [6150, 840, 6200, 900]}, {"index": 261, "bbox_2d": [6200, 780, 6250, 840]}, {"index": 262, "bbox_2d": [6200, 840, 6250, 900]}, {"index": 263, "bbox_2d": [6250, 780, 6300, 840]}, {"index": 264, "bbox_2d": [6250, 840, 6300, 900]}, {"index": 265, "bbox_2d": [6300, 780, 6350, 840]}, {"index": 266, "bbox_2d": [6300, 840, 6350, 900]}, {"index": 267, "bbox_2d": [6350, 780, 6400, 840]}, {"index": 268, "bbox_2d": [6350, 840, 6400, 900]}, {"index": 269, "bbox_2d": [6400, 780, 6450, 840]}, {"index": 270, "bbox_2d": [6400, 840, 6450, 900]}, {"index": 271, "bbox_2d": [6450, 780, 6500, 840]}, {"index": 272, "bbox_2d": [6450, 840, 6500, 900]}, {"index": 273, "bbox_2d": [6500, 780, 6550, 840]}, {"index": 274, "bbox_2d": [6500, 840, 6550, 900]}, {"index": 275, "bbox_2d": [6550, 780, 6600, 840]}, {"index": 276, "bbox_2d": [6550, 840, 6600, 900]}, {"index": 277, "bbox_2d": [6600, 780, 6650, 840]}, {"index": 278, "bbox_2d": [6600, 840, 6650, 900]}, {"index": 279, "bbox_2d": [6650, 780, 6700, 840]}, {"index": 280, "bbox_2d": [6650, 840, 6700, 900]}, {"index": 281, "bbox_2d": [6700, 780, 6750, 840]}, {"index": 282, "bbox_2d": [6700, 840, 6750, 900]}, {"index": 283, "bbox_2d": [6750, 780, 6800, 840]}, {"index": 284, "bbox_2d": [6750, 840,



Which building has a red and white striped antenna on its top?

A. The building with the Helaba logo B. The building with the DB logo C. The building with the Deutsche Bank logo D. The building with the Commerzbank logo

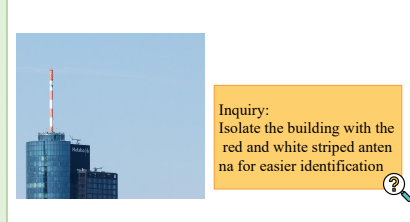
GPT-5 (thinking about images): In the image, the red and white striped antenna is clearly visible on top of the dark-blue skyscraper that has the "DB" logo near its top. None of the other buildings with logos (Helaba, Deutsche Bank, Commerzbank) have that red and white striped antenna. Final answer: B. The building with the DB logo. X

THYME (Code-based Thinking with Image):

<think> To determine which building has a red and white striped antenna on its top, we need to identify the building with this specific feature. Observing the image, the building with the Helaba logo has a red and white striped antenna on its top. This matches option A. The other buildings do not have this antenna feature. Therefore, the correct answer is A. </think>
<answer> A </answer> ✓

ViLAVT (chatting with images):

<think> To identify the building with the red and white striped antenna, it's important to concentrate on the specific antenna and examine the surrounding buildings. The antenna is situated on top of a tall building, and its distinctive color pattern makes it noticeable. However, the image includes numerous buildings, which can make pinpointing the right one somewhat complex without a closer examination. By cropping and zooming in on the area where the antenna is located, we can isolate the building and make the identification process easier.
The antenna appears to be on the right side of the image, near the center. Cropping this area will help focus on the building with the antenna. </think>
<tool>{"region": [{"index": 0, "bbox_2d": [1198, 500, 1996, 1200]}], "query": "Isolate the building with the red and white striped antenna for easier identification."} </tool>



<think> The building with the Helaba logo has a red and white striped antenna on top, as seen in the image. The other buildings do not have this particular antenna. </think>
<answer> A </answer> ✓

Figure 12. Second case (HRBench-4K, high-resolution perception). ViLAVT first performs targeted cropping and then correctly infers that the building has a red and white striped antenna. GPT-5 directly produces an incorrect answer, while Thyme outputs a response but does not provide an explicit reasoning process.



Where is the clock located in the room? A. Above the main seating area B. No clock in the room C. On the wall to the right of the main seating area D. On the wall to the left of the main seating area

GPT-5 (thinking about images): In the image, the main seating area is formed by the long tables and chairs in the center of the room. The clock is visible on the wall to the right-hand side of this seating area, above the wooden paneling and next to the windows. It is not above the center of the seating area, nor is it on the left. Final answer: C. On the wall to the right of the main seating area. 

THYME (Code-based Thinking with Image):

<think> To determine the location of the clock in the room, we need to observe its position relative to the main seating area. The clock is visible on the wall to the right side of the main seating area, as it is mounted on the wall adjacent to the chairs and tables. It is not positioned above the seating area or to the left of it. Therefore, option C is the correct choice. </think> <tool> <answer> C </answer> 

ViLAVT (chatting with images):

<think> To determine the location of the clock in the room, we first identify the main seating area which is the central part of the room with wooden tables and chairs and a green carpet. Then we locate the clock, a round wooden-framed clock with Roman numerals, which is mounted on the wall to the right of the main seating area. I need to identify the main seating area to establish a reference point for locating the clock. </think> <tool> {"region": [{"index": 0, "bbox_2d": [0, 1186, 2520, 2520]}], "query": "Locate the main seating area in the central part of the room."} </tool>



Inquiry:
Locate the main seating area in the central part of the room. 

<think> The main seating area is the central part of the room with wooden tables and chairs and a green carpet. After identifying the main seating area, the next step is to locate the clock. I need to find the clock to determine its position relative to the main seating area. </think> <tool> {"region": [{"index": 0, "bbox_2d": [1763, 677, 2221, 1047]}], "query": "Locate the clock on the wall to the right of the main seating area."} </tool>



Inquiry:
Locate the clock on the wall to the right of the main seating area. 

<think> The clock is mounted on the wall to the right of the main seating area. Based on the observations, I can now conclude the location of the clock. </think> <answer> C </answer> 

Figure 13. Third case (HRBench-4K, high-resolution perception). For reasoning about relative object positions, ViLAVT explicitly grounds the entities in the image and then derives the final answer. Both GPT-5 and Thyme arrive at the correct answer directly through text-based reasoning.



What is the purpose of the label in the red circle?

- The label indicates that the bottle costs an extra 10 cents in California
- The label is a discount coupon for purchasing the bottle
- The label indicates that consumers can get a refund of 10 cents if they return the bottle to a recycling center in California
- The label indicates a special tax that applies only to this brand of water in California

ViLAVT (chatting with images):

<think> The image contains a water bottle with a label in a red circle, which is a key detail for answering the question. However, the label's text is not clearly visible in the current image resolution. To accurately determine the purpose of the label, it is necessary to zoom in on the water bottle and its label. Cropping the image to focus on the water bottle will enhance the visibility of the label, making it easier to read and interpret. </think> <tool> {"region": [{"index": 0, "bbox_2d": [575, 975, 676, 1077]}], "query": "Enhance the visibility of the label on the water bottle to determine its purpose."} </tool>



Attention Visualization

Inquiry:
Enhance the visibility of the label on the water bottle to determine its purpose.



<think> The label in the red circle on the water bottle is a California state law label indicating that the bottle can be redeemed for a 10-cent refund if returned to a recycling center. This is a common practice in California to promote recycling and proper disposal of plastic bottles. </think>

ViLAVT (w/o inquiry):



Attention Visualization

Qwen2.5-VL-7B ViT



Attention Visualization

Figure 14. Attention map visualization on an example from HRBench-4K.

System Prompt

You are a helpful assistant. Your goal is to solve the problem in the provided image(s) based on the user's instruction. Proceed step by step, optionally using the zoom-in tool one or more times to examine key areas closely. Selected regions will be cropped and processed externally, then re-encoded with your query to extract critical details.

Tools

If needed, use the zoom-in tool one or more times to examine specific areas in detail.

Tool Format

Structure

```
{
  "region": [
    {
      "index": int, # Target image index to zoom in (0-based)
      "bbox_2d": list, # Format: [x1, y1, x2, y2], where (x1, y1)
      is top-left corner and (x2, y2) is bottom-right corner
    },
    ... # Additional regions (optional)
  ],
  "query": str # Description of what to look for in the selected regions
}
```

Parameters:

- region: List of dictionaries, each containing:
 - index: Integer, specifying which image to zoom in
 - bbox_2d: List of 4 integers [x1, y1, x2, y2] defining the region
- query: String describing the search target

Constraints:

- At least one region must be specified
- All coordinates must be within image boundaries
- x1 < x2 and y1 < y2 must be satisfied

Example:

```
<tool> {"region": [{"index": 0, "bbox_2d": [100, 200, 300, 400]}], "query": "Look for the red button"} </tool>
```

Figure 15. System prompt used in ViLAVT

User Prompt

The index of the provided image is 1

.....

The index of the provided image is `{max_index}`

These are `{n_frames}` images with indexed from 0 to `{max_index}`.
All images have size: width `{width}`, height `{height}`.

Question: `{question}`

If you need to zoom in for more details or examine specific regions, make tool call following the format:

```
<think> Your reasoning about where to look and why  </think>
<tool> \{\\"region": [\{\\"index": int, "bbox\_2d": [x1, y1, x2, y2]\}\}, ...], "query": str\}\} </tool>
```

If you have enough information to answer the original question:

```
<think> Your reasoning here.  </think>
<answer> Your final answer here. </answer>
```

- Note that `x1, y1, x2, y2` are the coordinates of the bounding box in the specified image by the index.
- You must strictly follow the above output format.
- In `<answer>`, provide **only** the final answer in the simplest required form:
 - For multiple-choice questions: output only the letter (e.g., `A, B, C`).
 - For yes/no questions: output only `Yes` or `No`.
 - For numerical answers: output only the number (e.g., `42, 3.14`).
 - Do not include explanations, units, punctuation, or extra words.

Figure 16. User prompt used in ViLAVT